Non-Cellular Satellite-UAV Networks for Wide-Area Internet of Things

Chengxiao Liu, Wei Feng, *Senior Member, IEEE,* Yunfei Chen, *Senior Member, IEEE,* Cheng-Xiang Wang, *Fellow, IEEE,* and Ning Ge, *Member, IEEE*

***Abstract*—In 5G and beyond networks, serving massive Internet of Things (IoT) devices in wide areas is critical. Due to the limited coverage of terrestrial cellular networks and severe channel environment of conventional satellite networks, it is beneficial to build a hybrid satellite-unmanned aerial vehicle (UAV) network. However, it is cost-ineffective to serve massive IoT devices using conventional cellular architectures. Thus, the consideration of non-cellular architecture is of great importance for hybrid satellite-UAV networks. To further cope with the spectrum scarcity problem under non-cellular architecture, building a cognitive satellite-UAV network (CSUN) will be desirable. In this paper, we focus on the comprehensive resource allocation of broadband CSUNs. A process-oriented optimization framework is proposed, which considers the whole flight process of UAVs in a large time scale under non-cellular architecture. The system performance is evaluated with the slowly-varying channel state information (CSI) under different conditions. Using the process-oriented optimization framework, the data transmission efficiency maximization problem and the minimum data transmission efficiency optimization problem are studied with energy constraints and interference power constraints. Using the time-sharing relaxation and feasible region relaxation techniques, the communication resources of CSUNs, including the subchannel usage, transmit power and hovering time, are jointly optimized in an iterative way. Simulation results demonstrate the superiority of the proposed algorithms over the existing algorithms.**

***Index Terms*—Cognitive satellite-UAV networks, massive access, non-cellular network, resource allocation, wide-area IoT.**

I. Introduction

In 5G and beyond networks, the demand for wide-area Internet of Things (IoT) with massive devices keeps increasing [1]–[3]. Thus, it is critical to support massive access in emerging terrestrial and satellite networks [4]. However, limited by the geographical environment, most IoT devices in wide areas, e.g., probe vehicles in oceans and mountains, are outside the coverage of terrestrial cellular networks [3]. Consequently, conventional cellular-based IoT technologies, such as Narrow Band-IoT (NB-IoT) and Long Range Radio (LoRa), are hard to be directly used for wide-area IoT devices. Besides, it is also challenging for current satellite networks to serve these devices, due to the high communication latency and severe channel environment [4].

To overcome these challenges, integrating unmanned aerial vehicles (UAVs) into satellite networks is widely regarded as an effective way. Nevertheless, existing works ignored the difficulties in building a broadband satellite-UAV network for massive IoT devices. In practice, massive IoT devices in wide areas are always unevenly distributed [5], [6], so that it is cost-ineffective to serve them based on conventional cellular architectures [7]. Hence, the design of non-cellular architecture is considered for efficient use of resources. Furthermore, to cope with the spectrum scarcity problem of broadband satellite-UAV networks under non-cellular architecture, it is beneficial to apply cognitive spectrum sharing techniques by building a cognitive satellite-UAV network (CSUN) [8]. Motivated by these observations, a comprehensive design of resource allocation strategies under non-cellular architecture is studied for CSUNs.

A. Related Works

Conventional IoT technologies are able to support massive access in urban scenarios [9]–[11]. In [9], emerging IoT networks were sufficiently surveyed, which pointed out that NB-IoT and LoRa are two typical technologies. The authors of [10] discussed the application of LoRa technique in smart cities. In [11], the architecture and applications of NB-IoT technique were surveyed. However, these technologies were designed under conventional cellular architecture, which are hard to allocate the limited communication resources to massive IoT devices in wide areas.

To serve the IoT devices outside the coverage of cellular networks, satellite communication is widely regarded as an enabling technique [12]. In satellite networks, spectrum scarcity is an everlasting problem. To handle this problem, cognitive spectrum sharing techniques were used to extend the spectrum of satellite networks [13]. In previous works, the spectrum sharing of satellite-terrestrial networks has been widely discussed, where interference mitigation techniques are crucial [14]–[16]. In [14], a hybrid analog-digital transmit beamforming technique was presented to mitigate the inter-system interference. The authors of [15] proposed a semi-adaptive beamforming scheme for hybrid satellite-terrestrial networks. In [16], an optimal beamforming technique was designed considering the imperfections of realistic satellite-terrestrial networks. However, these techniques did not consider the mobility of UAVs, so that the cognitive spectrum sharing techniques should be redesigned for CSUNs.

C. Liu, W. Feng (corresponding author) and Ning Ge are with the Beijing National Research Center for Information Science and Technology, Tsinghua University, Beijing 100084, China. (email: lcx17@mails.tsinghua.edu.cn, fengwei@tsinghua.edu.cn, gening@tsinghua.edu.cn).

Y. Chen is with the School of Engineering, University of Warwick, Coventry CV4 7AL, U.K. (e-mail: Yunfei.Chen@warwick.ac.uk).

C.-X. Wang is with the National Mobile Communications Research Laboratory, School of Information Science and Engineering, Southeast University, Nanjing 210096, China, and also with Purple Mountain Laboratories, Nanjing 211111, China. (e-mail: chxwang@seu.edu.cn).

Recent studies on UAV communications focused on the trajectory planning and resource allocation of UAVs [17]–[22]. In [17], the energy efficiency of UAVs was optimized, considering the energy consumption of the UAV propulsion. The authors of [18] proposed a placement strategy to optimize the reliability of UAV networks, on the basis of novel UAV channel models [19], [20]. In [21], an energy efficiency optimization method was proposed by jointly optimizing the transmit power and hovering time of the UAV swarm. The authors of [22] maximized the secrecy rate of a UAV-enabled network through resource allocation. Based on these works, the authors of [23], [24] further discussed the integration of UAVs with satellite networks. In [23], a coordinated multi-point transmission scheme was proposed for a UAV-aided cognitive satellite-terrestrial network, where the trajectory and transmit power of UAVs were jointly optimized under interference temperature constraints at different time slots. The authors of [24] investigated the optimal hovering altitude and transmit power of UAVs, which maximized the uplink sum rate under interference power constraints in a space-air-ground integrated IoT network.

Note that the works in [17], [18], [21]–[24] optimized the UAV-enabled networks under conventional cellular architectures, by means of trajectory planning and power allocation. However, these works are based on ideal assumptions, ignoring the intrinsic difficulties of building a broadband CSUN. On one hand, it is cost-ineffective to cover massive IoT devices by densely setting satellites and UAVs under conventional cellular architecture [7], which motivates us to design a non-cellular architecture for CSUNs. On the other hand, the resource allocation strategy of a broadband CSUN under non-cellular architecture is complicated, which has not been considered by existing works. Hence, it is of vital importance to discuss the comprehensive resource allocation strategy of broadband CSUNs under non-cellular architecture.

B. Main Contributions

In this paper, we focus on the resource allocation of CSUNs during the flight process of UAVs. Towards this end, a process-oriented optimization framework is proposed under non-cellular architecture. As a long period of time is required to complete the flight process, the process-oriented framework optimizes the resource allocation strategy in a large time scale. The main contributions are summarized as follows.

- We establish a process-oriented model of CSUNs, which means that the UAV flight process is studied in a large time scale. Furthermore, to be more realistic, both the imperfect acquisition of channel state information (CSI) and the energy constraints of the UAV swarm are considered. Besides, the interference constraints under non-cellular architecture are also accounted for. The path loss and shadowing of the UAV channel is generated based on the realistic geographical environment using channel models recommended by ITU-R [25], [26].
- A data transmission efficiency maximization problem is formulated based on the process-oriented model under non-cellular architecture. The original problem is then simplified and decomposed into three subproblems, where the subchannel usage, transmit power and hovering time are optimized separately by using the time-sharing relaxation technique. Based on the solutions to the subproblems, the original problem is solved in an iterative way.
- To further improve the coverage ability of CSUNs, we reformulate the original objective function to a max-min one. The solution to the newly derived minimum data transmission efficiency optimization problem is also proposed. Then, the max-min optimization problem is decomposed into three subproblems. The subproblems are solved using feasible region relaxation techniques. Using these techniques, the original max-min problem is also solved in an iterative way.

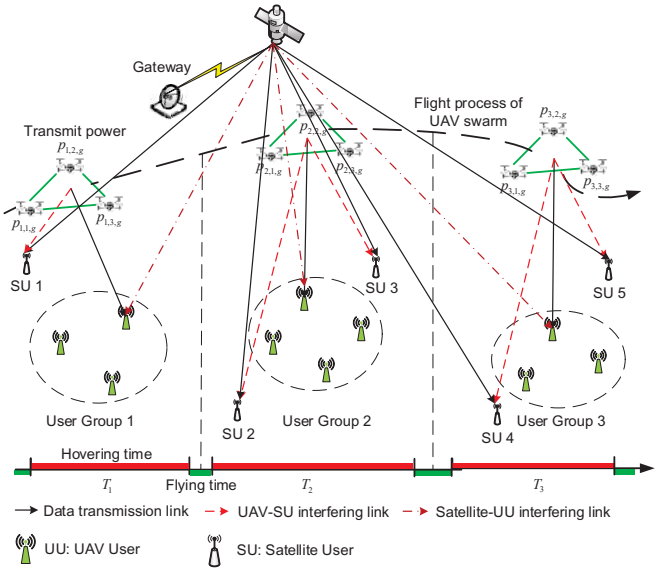

Fig. 1. Illustration of a general CSUN under non-cellular architecture, where the g-th subchannel is used.

The rest of this paper is organized as follows. We introduce the system model and the channel model in Section II. In Section III, the data transmission efficiency maximization problem is formulated and solved. We further discuss the minimum data transmission efficiency optimization problem and its solution in Section IV. Section V presents simulation results and discussions, and the conclusions of this work are given in Section VI.

II. System Model

We consider a general CSUN under a non-cellular architecture, which consists of N_U UAV users (UUs) that are served by the UAV swarm during a flight process, and N_s satellite users (SUs) that are served by the satellite, as shown in Fig. 1. Without loss of generality, we assume that each UU is equipped with M antennas, and each SU has single antenna. To reduce the cost of UAV communications, the UAV swarm is assumed with K single-antenna UAVs, which can serve UUs in a coordinated manner. Besides, the UAV swarm works in a stable and energy-efficient *hover-to-transmit* mode [27], [28] to provide downlink services, i.e., the UAV swarm will hover above a group of UUs and transmit data for some time, and

then fly to the next group of UUs to serve them. This process is repeated until all service demands from UUs are satisfied.

In CSUNs under non-cellular architecture, the UAV swarm and the satellite use the same frequency band to serve users. We assume the frequency band can be divided into G subchannels, which are shared by all UUs and SUs. To serve massive UUs with limited spectrum resources, we divide the UUs into N groups [4], and the n-th group of users is served by the UAV swarm at the n-th time slot. Moreover, we assume that the n-th group has U_n UUs, where $\sum_{n=1}^{N} U_n = N_U$ is naturally satisfied. Accordingly, the received signal of the u-th UU in the n-th user group using the g-th subchannel can be expressed as

$$\mathbf{r}_{n,u,g} = \mathbf{H}_{n,u,g}\mathbf{s}_{n,u,g} + \mathbf{q}_{n,u,g} \tag{1}$$

where $n \in \{1,...,N\}$, $u \in \{1,...,U_n\}$, $g \in \{1,...,G\}$, $\mathbf{H}_{n,u,g} \in \mathbb{C}^{M\times K}$ denotes the channel matrix, $\mathbf{s}_{n,u,g} \in \mathbb{C}^{K}$ is the transmit signal of K UAVs and $\mathbf{q}_{n,u,g} \in \mathbb{C}^{K}$ denotes the additive white Gaussian noise following $\mathcal{CN}(\mathbf{0}_M, \sigma^2\mathbf{I}_M)$, where $\mathbf{0}_M \in \mathbb{C}^{M}$ and $\mathbf{I}_M \in \mathbb{C}^{M\times M}$ are the all-zero vector and the identity matrix respectively.

In (1), we consider a realistic UAV channel model, which includes both fast and slow elements of a realistic UAV channel [18], given by

$$\mathbf{H}_{n,u,g} = \mathbf{S}_{n,u,g}\mathbf{L}_{n,u,g}. \tag{2}$$

In (2), the components of $\mathbf{S}_{n,u,g} \in \mathbb{C}^{M\times K}$ are i.i.d. standard complex Gaussian random variables. These variables can describe the fast fading (e.g. multipath fading) of UAV channel. Besides, $\mathbf{L}_{n,u,g} = \text{diag}\{l_{n,u,1,g},...,l_{n,u,K,g}\} \in \mathbb{C}^{K\times K}$ is a diagonal matrix which can describe the slowly-varying parameters of the UAV channel. To be more realistic, we use the space-air channel models in Recommendation ITU-R P.525 and Recommendation ITU-R P.676-10 to generate $\mathbf{L}_{n,u,g}$ according to the geographical information [25], [26]. Using this channel model, both the line-of-sight (LOS) links and the non-line-of-sight (NLOS) links between UAVs and users can be appropriately described.

More importantly, the consideration of the realistic channel model will introduce additional challenges to CSUNs. In previous works [29], [30], the UAV trajectory and communication were jointly designed based on a simplified position-related channel model. However, the UAV trajectory is actually coupled with the inter-system interference under the influence of varying channel environment in CSUNs, which is too complicated to be analyzed. To simplify the mathematical analysis, we assume the trajectory of UAVs can be designed prior to the flight [21], and the locations of users are also known, e.g., provided by global positioning system [22]. Hence, we can acquire the slowly-varying large-scale CSI, i.e., $\mathbf{L}_{n,u,g}$ in (2), prior to the flight. On the other hand, $\mathbf{S}_{n,u,g}$ in (2) varies fast and can not be precisely acquired by UAVs [21]. We assume the transmitter only knows the distribution of $\mathbf{S}_{n,u,g}$. Such design actually focuses on the long-term behavior of the whole flight process, which indicates that the system model is process-oriented.

It is worth noting that the communication resources are allocated to UAVs in docking stations using large-scale CSI, which can realize the coordination among UAVs in an offline way. Denoting $\mathbf{P}_{n,g} = \text{diag}\{p_{n,1,g},...,p_{n,K,g}\}$ as the transmit power of the UAV swarm when it is hovering above the n-th user group using the g-th subchannel, the downlink rate of UU can be written as

$$R_{n,u,g} = \log_2\text{det}\left(\mathbf{I}_M + \frac{1}{\sigma^2}\mathbf{S}_{n,u,g}\mathbf{L}_{n,u,g}\mathbf{P}_{n,g}\mathbf{L}_{n,u,g}\mathbf{S}_{n,u,g}^H\right). \tag{3}$$

Furthermore, to describe the data transmission efficiency of the UAV swarm, the subchannel usage and hovering time of UAVs should be regarded. We define $x_{n,u,g} \in \{0,1\}$ as indicator variables for subchannel usage, where $x_{n,u,g} = 1$ means that the g-th subchannel is occupied by the u-th UU of the n-th user group. We also define T_n as the hovering time of the UAV swarm at the n-th user group. Based on (3), the data transmission efficiency of the UAV swarm is written as

$$\mathcal{D}(\mathbf{P},\mathbf{T},\mathbf{x}) = \sum_{n=1}^{N}\sum_{u=1}^{U_n}\sum_{g=1}^{G} x_{n,u,g}T_nR_{n,u,g} \tag{4}$$

where $\mathbf{P} = \{\mathbf{P}_{n,g} \ \forall n,g\}$ is the set of transmit power, $\mathbf{T} = (T_1,...,T_N)^T$ is the hovering time of the UAV swarm, $\mathbf{x} = \{x_{n,u,g} \ \forall n,u,g\}$ is the set of indicator variables. As the instantaneous CSI, i.e., $\mathbf{S}_n$, is not known, we consider the *ergodic* data transmission efficiency given by [31]

$$\mathcal{D}_e(\mathbf{P},\mathbf{T},\mathbf{x}) = \mathbf{E}_{\mathbf{S}}\{\mathcal{D}(\mathbf{P},\mathbf{T},\mathbf{x})\} \tag{5}$$

where $\mathbf{S} = \{\mathbf{S}_{n,u,g}, \forall n,u,g\}$ is the set of small-scale channel parameters, $\mathbf{E}_{\mathbf{S}}$ represents the expectation with respect to small-scale parameters, which is used for evaluating the performance of the whole flight process in a large time scale.

In CSUNs under non-cellular architecture, N_s single-antenna SUs will be interfered by the transmit signal of the UAV swarm when a subchannel is simultaneously used by UUs and SUs. Besides, there also exists interference between the satellite and UUs. Regarding the high latency of satellite communications [32], it is hard to adjust the signal of satellites instantaneously, so that the interference between the satellite and UUs is regarded to be unchanged. Hence, we ignore the interference between the satellite and UUs for simplicity, and focus on the interference between the UAV swarm and SUs. Without loss of generality, we assume the interfering channel also satisfies the UAV channel model in (2). We can characterize the g-th subchannel between the UAV swarm and the i-th SU at the n-th time slot by

$$\mathbf{h}_{n,i,g} = \mathbf{s}_{n,i,g}\mathbf{L}_{n,i,g} \tag{6}$$

where $i \in \{1,...,N_s\}$, the components of $\mathbf{s}_{n,i,g} = (s_{n,i,1,g},...,s_{n,i,K,g}) \in \mathbb{C}^{1\times K}$ are also i.i.d standard complex Gaussian random variables. Following the same line of reasoning as (4) and (5), we can formulate the interference power of the UAV swarm at the i-th SU as

$$\mathcal{I}_{n,i} = \sum_{u=1}^{U_n}\sum_{g=1}^{G} x_{n,u,g}y_{n,i,g} \mathbf{E}_{\mathbf{s}_{n,i,g}}\left\{\mathbf{s}_{n,i,g}\mathbf{L}_{n,i,g}\mathbf{P}_{n,g}\mathbf{L}_{n,i,g}\mathbf{s}_{n,i,g}^H\right\}$$

$$= \sum_{u=1}^{U_n}\sum_{k=1}^{K}\sum_{g=1}^{G} x_{n,u,g} y_{n,i,g} l_{n,i,k,g}^2 p_{n,k,g} \tag{7}$$

when the UAV swarm is hovering above the n-th user group, where $k \in \{1, ..., K\}$ denotes the identifier of UAV, $\mathbf{y} = \{y_{n,i,g} \in \{0,1\} \ \ \forall n, i, g\}$ shows that the i-th SU will use the g-th subchannel at the n-th time slot if $y_{n,i,g} = 1$, $\mathbf{E}_{\mathbf{s}_{n,i,g}}$ denotes the expectation with repect to small-scale parameters.

Moreover, the UAV swarm in CSUN is encountering practical constraints due to the limited on-board energy of UAVs. Specifically, the constraints of the total energy, the transmit power and the hovering time of UAVs should be jointly considered. For energy constraints, when the UAVs are working in the hover-to-transmit mode, both the propulsion energy and the communication energy are important [33]. In this model, as the trajectory of UAVs is assumed to be known prior to the flight, the propulsion energy is assumed to be constant accordingly. Hence, we can formulate the energy constraints of the UAV swarm as [21]

$$\sum_{n=1}^{N}\sum_{u=1}^{U_n}\sum_{g=1}^{G} x_{n,u,g} p_{n,k,g} T_n \le E_k \ \ \forall k \tag{8}$$

where the subchannel usage indicator $\mathbf{x}$ is regarded in (8) so that the transmit energy would be allocated to the subchannels which are being used by UUs. Such design can save the energy consumption of UAVs, because the communication energy would not be allocated to unused subchannels. Accordingly, the transmit power constraints are derived as

$$\sum_{u=1}^{U_n}\sum_{g=1}^{G} x_{n,u,g} p_{n,k,g} \le p_{max} \ \ \forall n, k. \tag{9}$$

Besides, the hovering time of the UAV swarm should also be carefully regarded [21]. The hovering time constraints are formulated by

$$\sum_{n=1}^{N} T_n \le T_{total} \tag{10}$$

$$T_n \le T_{max} \ \ \forall n \tag{11}$$

where (10) denotes the constraint of total hovering time and (11) is the constraint of the maximum hovering time.

III. Process-oriented Data Transmission Efficiency Maximization

In this section, we propose an algorithm to maximize the data transmission efficiency of the UAV swarm based on the process-oriented model. The proposed algorithm jointly considers the subchannel allocation, the transmit power allocation and the hovering time scheduling to optimize the overall data transmission efficiency. The data transmission efficiency maximization problem is formulated as

$$\max_{\mathbf{P},\mathbf{T},\mathbf{x}} \ \mathcal{D}_e(\mathbf{P}, \mathbf{T}, \mathbf{x}) \tag{12a}$$

$$s.t. \ \ \sum_{u=1}^{U_n}\sum_{k=1}^{K}\sum_{g=1}^{G} x_{n,u,g} y_{n,i,g} l_{n,i,k,g}^2 p_{n,k,g} \le \epsilon_p \ \ \forall n, i \tag{12b}$$

$$\sum_{n=1}^{N}\sum_{u=1}^{U_n}\sum_{g=1}^{G} x_{n,u,g} p_{n,k,g} T_n \le E_k \ \ \forall k \tag{12c}$$

$$\sum_{u=1}^{U_n}\sum_{g=1}^{G} x_{n,u,g} p_{n,k,g} \le p_{max} \ \ \forall n, k \tag{12d}$$

$$\sum_{n=1}^{N} T_n \le T_{total} \tag{12e}$$

$$T_n \le T_{max} \ \ \forall n \tag{12f}$$

$$\sum_{u=1}^{U_n} x_{n,u,g} \le 1 \ \ \forall n, g \tag{12g}$$

$$x_{n,u,g} \in \{0,1\} \ p_{n,k,g} \ge 0 \ T_n \ge 0 \ \ \forall n, u, k, g \tag{12h}$$

where (12b)–(12f) are practical constraints of the UAV swarm as was discussed in (7)–(11), ϵ_p denotes the interference power threshold, and (12g) means that a subchannel can only be allocated to one user. The problem in (12) is a mixed-integer nonlinear programming (MINLP) problem, which is not convex and hard to be solved directly. In this section, we propose a method to simplify (12) and then propose an iterative algorithm to solve it.

A. Problem Transformation

We utilize the techniques proposed in [21] to simplify (12). First, we formulate a new objective function $\mathcal{D}_a(\mathbf{P}, \mathbf{T}, \mathbf{x}, \mathbf{w})$ as, which can closely approximate $\mathcal{D}_e(\mathbf{P}, \mathbf{T}, \mathbf{x})$ without expectation,

$$\mathcal{D}_a(\mathbf{P}, \mathbf{T}, \mathbf{w}, \mathbf{x}) = \sum_{n=1}^{N}\sum_{u=1}^{U_n}\sum_{g=1}^{G} x_{n,u,g} T_n R_a(\mathbf{P}_{n,g}, w_{n,u,g}) \tag{13}$$

where

$$R_a(\mathbf{P}_{n,g}, w_{n,u,g}) = \sum_{k=1}^{K} \log_2\left(1 + \frac{M l_{n,u,k,g}^2 p_{n,k,g}}{w_{n,u,g}\sigma^2}\right) + M\left[\log_2 w_{n,u,g} - \log_2 e(1 - w_{n,u,g}^{-1})\right] \tag{14}$$

and $\mathbf{w} = \{w_{n,u,g} \ \ \forall n, u, g\}$ is a set of slack variables which satisfies

$$w_{n,u,g} = 1 + \sum_{k=1}^{K} \frac{l_{n,u,k,g}^2 p_{n,k,g}}{\sigma^2 + M l_{n,u,k,g}^2 p_{n,k,g} w_{n,u,g}^{-1}}. \tag{15}$$

The equation in (14) shows that the approximated rate is a sum of the modified data rate and the compensation term which is related to the slack variable $\mathbf{w}$. The equations in (15) indicate that $\mathbf{w}$ is an implicit function with respect to $\mathbf{P}$, so that $\mathbf{w}$ is not an optimization variable and the optimization of $\mathbf{P}$ is more important. Besides, the accuracy of this approximation technique has been discussed in [31] in details. With (13) and (15), (12) is transformed to

$$\max_{\mathbf{P},\mathbf{T},\mathbf{x}} \ \mathcal{D}_a(\mathbf{P}, \mathbf{T}, \mathbf{w}, \mathbf{x}) \tag{16a}$$

$$s.t. \ \ \sum_{u=1}^{U_n}\sum_{k=1}^{K}\sum_{g=1}^{G} x_{n,u,g} y_{n,i,g} l_{n,i,k,g}^2 p_{n,k,g} \le \epsilon_p \ \ \forall n, i \tag{16b}$$

$$\sum_{n=1}^{N}\sum_{u=1}^{U_n}\sum_{g=1}^{G} x_{n,u,g}p_{n,k,g}T_n \le E_k \quad \forall k \tag{16c}$$

$$\sum_{u=1}^{U_n}\sum_{g=1}^{G} x_{n,u,g}p_{n,k,g} \le p_{max} \quad \forall n,k \tag{16d}$$

$$\sum_{n=1}^{N} T_n \le T_{total} \tag{16e}$$

$$T_n \le T_{max} \quad \forall n \tag{16f}$$

$$\sum_{u=1}^{U_n} x_{n,u,g} \le 1 \quad \forall n,g \tag{16g}$$

$$w_{n,u,g} = 1 + \sum_{k=1}^{K} \frac{l^2_{n,u,k,g}p_{n,k,g}}{\sigma^2 + Ml^2_{n,u,k,g}p_{n,k,g}w^{-1}_{n,u,g}} \quad \forall n,u,g \tag{16h}$$

$$x_{n,u,g} \in \{0,1\}\ p_{n,k,g} \ge 0\ T_n \ge 0 \quad \forall n,u,k,g \tag{16i}$$

where the new constraint (16h) is introduced by the coupling between $\mathbf{P}$ and $\mathbf{w}$ according to (15).

B. Problem Decomposition

The new problem in (16) is not convex, due to the coupling between $\mathbf{P}$, $\mathbf{T}$ and $\mathbf{x}$. To solve this problem, we decompose (16) into three subproblems. In the first subproblem, $\mathbf{x}$ is the optimization variable, while $\mathbf{P}$ and $\mathbf{T}$ are regarded as constants. This subproblem is an integer linear programming (ILP) problem, and its solution is referred to as the subchannel allocation scheme. Moreover, in the second subproblem, $\mathbf{P}$ is the optimization variable while $\mathbf{T}$ and $\mathbf{x}$ are regarded as constants. Its solution is referred to as the coordinated power allocation scheme. Besides, for the third subproblem, $\mathbf{T}$ is the optimization variable while $\mathbf{P}$ and $\mathbf{x}$ are regarded as constants. Its solution is referred to as the hovering time scheduling scheme.

Denoting the iteration index as r, we can first formulate the subchannel allocation scheme as

$$\max_{\mathbf{x}^r}\ \mathcal{D}_a(\mathbf{P}^{r-1},\mathbf{T}^{r-1},\mathbf{w}^{r-1},\mathbf{x}^r) \tag{17a}$$

$$s.t.\ \sum_{u=1}^{U_n}\sum_{k=1}^{K}\sum_{g=1}^{G} x^r_{n,u,g}y_{n,i,g}l^2_{n,i,k,g}p^{r-1}_{n,k,g} \le \epsilon_p \quad \forall n,i \tag{17b}$$

$$\sum_{n=1}^{N}\sum_{u=1}^{U_n}\sum_{g=1}^{G} x^r_{n,u,g}p^{r-1}_{n,k,g}T^{r-1}_n \le E_k \quad \forall k \tag{17c}$$

$$\sum_{u=1}^{U_n}\sum_{g=1}^{G} x^r_{n,u,g}p^{r-1}_{n,k,g} \le p_{max} \quad \forall n,k \tag{17d}$$

$$\sum_{u=1}^{U_n} x^r_{n,u,g} \le 1 \quad \forall n,g \tag{17e}$$

$$x^r_{n,u,g} \in \{0,1\} \quad \forall n,u,g. \tag{17f}$$

Then, we can derive the power allocation subproblem as

$$\max_{\mathbf{P}^r}\ \mathcal{D}_a(\mathbf{P}^r,\mathbf{T}^{r-1},\mathbf{w}^r,\mathbf{x}^r) \tag{18a}$$

$$s.t.\ \sum_{u=1}^{U_n}\sum_{k=1}^{K}\sum_{g=1}^{G} x^r_{n,u,g}y_{n,i,g}l^2_{n,i,k,g}p^r_{n,k,g} \le \epsilon_p \quad \forall n,i \tag{18b}$$

$$\sum_{n=1}^{N}\sum_{u=1}^{U_n}\sum_{g=1}^{G} x^r_{n,u,g}p^r_{n,k,g}T^{r-1}_n \le E_k \quad \forall k \tag{18c}$$

$$\sum_{u=1}^{U_n}\sum_{g=1}^{G} x^r_{n,u,g}p^r_{n,k,g} \le p_{max} \quad \forall n,k \tag{18d}$$

$$w^r_{n,u,g} = 1 + \sum_{k=1}^{K} \frac{l^2_{n,u,k,g}p^r_{n,k,g}}{\sigma^2 + Ml^2_{n,u,k,g}p^r_{n,k,g}(w^r_{n,u,g})^{-1}} \quad \forall n,u,g \tag{18e}$$

$$p^r_{n,k,g} \ge 0 \quad \forall n,k,g \tag{18f}$$

and we can derive the hovering time scheduling subproblem as

$$\max_{\mathbf{T}^r}\ \mathcal{D}_a(\mathbf{P}^r,\mathbf{T}^r,\mathbf{w}^r,\mathbf{x}^r) \tag{19a}$$

$$s.t.\ \sum_{n=1}^{N}\sum_{u=1}^{U_n}\sum_{g=1}^{G} x^r_{n,u,g}p^r_{n,k,g}T^r_n \le E_k \quad \forall k \tag{19b}$$

$$\sum_{n=1}^{N} T^r_n \le T_{total} \tag{19c}$$

$$0 \le T^r_n \le T_{max} \quad \forall n. \tag{19d}$$

It is easy to observe that the subproblem in (19) is a linear programming algorithm, which can be directly solved using conventional linear optimization tools [34]. Hence, we focus on deriving the solution to (17) and (18), and the methods will be described in Section III.C and Section III.D.

C. Subchannel Allocation

In this section, we propose a method to solve the subchannel allocation subproblem (17). As (17) is an ILP problem, it is hard to be solved directly. We use the time-sharing relaxation technique to solve this problem [35]. Using time-sharing relaxation technique, the optimization variables $x^r_{n,u,g} \in \{0,1\}$ are relaxed to continuous ones $z^r_{n,u,g} \in [0,1]$. Actually, $z^r_{n,u,g}$ can be regarded as the fraction of time that is used by the u-th UU in the n-th user group at the g-th subchannel. Hence, the original problem (17) is transformed to

$$\max_{\mathbf{z}^r}\ \mathcal{D}_a(\mathbf{P}^{r-1},\mathbf{T}^{r-1},\mathbf{w}^{r-1},\mathbf{z}^r) \tag{20a}$$

$$s.t.\ \sum_{u=1}^{U_n}\sum_{k=1}^{K}\sum_{g=1}^{G} z^r_{n,u,g}y_{n,i,g}l^2_{n,i,k,g}p^{r-1}_{n,k,g} \le \epsilon_p \quad \forall n,i \tag{20b}$$

$$\sum_{n=1}^{N}\sum_{u=1}^{U_n}\sum_{g=1}^{G} z^r_{n,u,g}p^{r-1}_{n,k,g}T^{r-1}_n \le E_k \quad \forall k \tag{20c}$$

$$\sum_{u=1}^{U_n}\sum_{g=1}^{G} z^r_{n,u,g}p^{r-1}_{n,k,g} \le p_{max} \quad \forall n,k \tag{20d}$$

$$\sum_{u=1}^{U_n} z^r_{n,u,g} \le 1 \quad \forall n,g \tag{20e}$$

$$0 \le z^r_{n,u,g} \le 1 \quad \forall n,u,g. \tag{20f}$$

From (20), we can see that the original ILP problem is converted to a linear programming problem, which can be solved using conventional linear optimization tools [34]. However, the key point is how to recover the original integer variables with continuous variables, i.e., calculate $\mathbf{x}^r$ using $\mathbf{z}^r$.

To handle this problem, we formulate the Lagrangian dual function of (20) as

$$\begin{aligned}
&L(\mathbf{z}^r, \boldsymbol{\lambda}, \boldsymbol{\mu}, \boldsymbol{\gamma}, \boldsymbol{\zeta}) = \mathcal{D}_a(\mathbf{P}^{r-1}, \mathbf{T}^{r-1}, \mathbf{w}^{r-1}, \mathbf{z}^r) \\
&+ \sum_{n=1}^{N}\sum_{i=1}^{N_s} \lambda_{n,i}(\epsilon_p - \sum_{u=1}^{U_n}\sum_{k=1}^{K}\sum_{g=1}^{G} z^r_{n,u,g} y_{n,i,g} l^2_{n,i,k,g} p^{r-1}_{n,k,g}) \\
&+ \sum_{k=1}^{K} \mu_k(E_k - \sum_{n=1}^{N}\sum_{u=1}^{U_n}\sum_{g=1}^{G} z^r_{n,u,g} p^{r-1}_{n,k,g} T^{r-1}_n) \\
&+ \sum_{n=1}^{N}\sum_{k=1}^{K} \gamma_{n,k}(p_{max} - \sum_{u=1}^{U_n}\sum_{g=1}^{G} z^r_{n,u,g} p^{r-1}_{n,k,g}) \\
&+ \sum_{n=1}^{N}\sum_{g=1}^{G} \zeta_{n,g}(1 - \sum_{u=1}^{U_n} z^r_{n,u,g})
\end{aligned} \tag{21}$$

where $\boldsymbol{\lambda}, \boldsymbol{\mu}, \boldsymbol{\gamma}, \boldsymbol{\zeta}$ are Lagrangian multipliers. Let us define

$$f(\boldsymbol{\lambda}, \boldsymbol{\mu}, \boldsymbol{\gamma}, \boldsymbol{\zeta}) = \sup_{\mathbf{z}^r} L(\mathbf{z}^r, \boldsymbol{\lambda}, \boldsymbol{\mu}, \boldsymbol{\gamma}, \boldsymbol{\zeta}). \tag{22}$$

Then, we can derive the Lagrangian dual problem of (20) as

$$\min_{\boldsymbol{\lambda}, \boldsymbol{\mu}, \boldsymbol{\gamma}, \boldsymbol{\zeta}} \ f(\boldsymbol{\lambda}, \boldsymbol{\mu}, \boldsymbol{\gamma}, \boldsymbol{\zeta}) \tag{23a}$$

$$s.t. \ \lambda_{n,i} \geq 0 \ \mu_k \geq 0 \ \gamma_{n,k} \geq 0 \ \zeta_{n,g} \geq 0 \quad \forall n, i, k, g \tag{23b}$$

The original linear optimization problem in (20) can be solved after the solution to (23) is given. Although such solution is still a continuous one, the integer variable $\mathbf{x}^r$ can be derived based on the formulation of (23). Further by using the Karush-Kuhn-Tucker (KKT) conditions [34], we can give a strategy to recover the original integer variable $\mathbf{x}^r$ and update the Lagrangian multipliers at every step of the iteration. Firstly, we define

$$\begin{aligned}
V_{n,u,g} &= \frac{\partial L(\mathbf{z}^r, \boldsymbol{\lambda}, \boldsymbol{\mu}, \boldsymbol{\gamma}, \boldsymbol{\zeta})}{\partial z^r_{n,u,g}} + \zeta_{n,g} \\
&= T_n R_a(\mathbf{P}_{n,g}, w_{n,u,g}) - \sum_{i=1}^{N_s}\sum_{k=1}^{K} \lambda_{n,i} y_{n,i,g} l^2_{n,i,k,g} p^{r-1}_{n,k,g} \\
&- \sum_{k=1}^{K} \mu_k p^{r-1}_{n,k,g} T^{r-1}_n - \sum_{k=1}^{K} \gamma_{n,k} p^{r-1}_{n,k,g}.
\end{aligned} \tag{24}$$

In fact, a new objective function is defined in (24). The newly defined function is a sum of the original data transmission efficiency and the penalty terms. The consideration of penalty terms can guarantee that all the constraints of the optimization problem can be satisfied. Then, $\mathbf{x}^r$ is recovered by the maximum $V_{n,u,g}$ using a similar technique in [35], i.e.,

$$x^r_{n,u^*,g} = \begin{cases} 1, & u^* = \arg\max_u \{V_{n,u,g} \quad \forall n, g\} \\ 0, & \text{else.} \end{cases} \tag{25}$$

Denoting the iteration index as t, the Lagrangian multipliers are updated using the subgradiant method by

$$\lambda^t_{n,i} = \left[\lambda^{t-1}_{n,i} + \delta^t_1 \frac{\partial L(\mathbf{z}^r, \boldsymbol{\lambda}, \boldsymbol{\mu}, \boldsymbol{\gamma}, \boldsymbol{\zeta})}{\partial \lambda_{n,i}}\right]^+ \tag{26}$$

Algorithm 1 Algorithm to solve (17)

Input: ϵ_p, $\{E_k, k = 1 \sim K\}$, p_{max}, $\mathbf{T}^{r-1}$, $\mathbf{P}^{r-1}$, δ^1_1, δ^1_2, δ^1_3;

Initialization: $\boldsymbol{\lambda}^0 = \mathbf{0}$, $\boldsymbol{\mu}^0 = \mathbf{0}$,$\boldsymbol{\gamma}^0 = \mathbf{0}$, $t = 1$;
repeat
  Calculate $V_{n,u,g}$ using (24);
  Update $\mathbf{x}^r$ using (25);
  Update $\boldsymbol{\lambda}^t$ using (26), where $\delta^t_1 = \delta^1_1/t$;
  Update $\boldsymbol{\mu}^t$ using (27), where $\delta^t_2 = \delta^1_2/t$;
  Update $\boldsymbol{\gamma}^t$ using (28), where $\delta^t_3 = \delta^1_3/t$;
  $t = t + 1$;
until $\mathbf{x}^r$ converges;

Output: $\mathbf{x}^r$.

$$\mu^t_k = \left[\mu^{t-1}_k + \delta^t_2 \frac{\partial L(\mathbf{z}^r, \boldsymbol{\lambda}, \boldsymbol{\mu}, \boldsymbol{\gamma}, \boldsymbol{\zeta})}{\partial \mu_k}\right]^+ \tag{27}$$

$$\gamma^t_{n,k} = \left[\gamma^{t-1}_{n,k} + \delta^t_3 \frac{\partial L(\mathbf{z}^r, \boldsymbol{\lambda}, \boldsymbol{\mu}, \boldsymbol{\gamma}, \boldsymbol{\zeta})}{\partial \gamma_{n,k}}\right]^+ \tag{28}$$

where $[\cdot]^+ = \max(\cdot, 0)$ and

$$\begin{aligned}
\frac{\partial L(\mathbf{z}^r, \boldsymbol{\lambda}, \boldsymbol{\mu}, \boldsymbol{\gamma}, \boldsymbol{\zeta})}{\partial \lambda_{n,i}} =& \epsilon_p \\
&- \sum_{u=1}^{U_n}\sum_{k=1}^{K}\sum_{g=1}^{G} x^r_{n,u,g} y_{n,i,g} l^2_{n,i,k,g} p^{r-1}_{n,k,g}
\end{aligned} \tag{29}$$

$$\frac{\partial L(\mathbf{z}^r, \boldsymbol{\lambda}, \boldsymbol{\mu}, \boldsymbol{\gamma}, \boldsymbol{\zeta})}{\partial \mu_k} = E_k - \sum_{n=1}^{N}\sum_{u=1}^{U_n}\sum_{g=1}^{G} x^r_{n,u,g} p^{r-1}_{n,k,g} T^{r-1}_n \tag{30}$$

$$\frac{\partial L(\mathbf{z}^r, \boldsymbol{\lambda}, \boldsymbol{\mu}, \boldsymbol{\gamma}, \boldsymbol{\zeta})}{\partial \gamma_{n,k}} = p_{max} - \sum_{u=1}^{U_n}\sum_{g=1}^{G} x^r_{n,u,g} p^{r-1}_{n,k,g}. \tag{31}$$

Based on (24)–(31), the subchannel allocation method is summarized in Algorithm 1.

D. Coordinated Power Allocation

In this section, we give the solution to (18). It has been proved in [31] that the objective function in (18a) is convex when both $\mathbf{P}^r$ and $\mathbf{w}^r$ satisfy (18e). However, (18e) shows that the coupling between $\mathbf{P}^r$ and $\mathbf{w}^r$ is too complicated, so that it is hard to solve (18) directly with low computational complexity. To reduce the complexity, we propose to relax (18e) and solve (18) in a iterative way. Denoting the iteration index as j, (18) can be reformulated as

$$\max_{\mathbf{P}^j} \ \mathcal{D}_a(\mathbf{P}^j, \mathbf{T}^{r-1}, \mathbf{w}^{j-1}, \mathbf{x}^r) \tag{32a}$$

$$s.t. \quad \sum_{u=1}^{U_n}\sum_{k=1}^{K}\sum_{g=1}^{G} x^r_{n,u,g} y_{n,i,g} l^2_{n,i,k,g} p^j_{n,k,g} \leq \epsilon_p \quad \forall n, i \tag{32b}$$

$$\sum_{n=1}^{N}\sum_{u=1}^{U_n}\sum_{g=1}^{G} x^r_{n,u,g} p^j_{n,k,g} T^{r-1}_n \leq E_k \quad \forall k \tag{32c}$$

$$\sum_{u=1}^{U_n}\sum_{g=1}^{G} x^r_{n,u,g} p^j_{n,k,g} \leq p_{max} \quad \forall n, k \tag{32d}$$

$$p^j_{n,k,g} \geq 0 \quad \forall n,k,g \tag{32e}$$

where $\mathbf{w}^{j-1}$ is regarded as a constant in (32). After $\mathbf{P}^j$ is obtained, we can update $\mathbf{w}^j$ by

$$w^j_{n,u,g} = 1 + \sum_{k=1}^{K} \frac{l^2_{n,u,k,g} p^j_{n,k,g}}{\sigma^2 + M l^2_{n,u,k,g} p^j_{n,k,g} (w^j_{n,u,g})^{-1}} \quad \forall n,u,g \tag{33}$$

Based on the solution to (32) and (33), we can derive the solution to (18) using Algorithm 2.

However, the convergence of Algorithm 2 is hard to be proved directly. To elaborate this issue, we use the variable substitution technique proposed in [21]. We substitute $w^r_{n,u,g} = e^{v^r_{n,u,g}}$ into (18), so that (18) is rewritten as

$$\max_{\mathbf{P}^r} \min_{\mathbf{v}^r} \ \mathcal{D}_a(\mathbf{P}^r, \mathbf{T}^{r-1}, \mathbf{v}^r, \mathbf{x}^r) \tag{34a}$$

$$s.t. \quad \sum_{u=1}^{U_n} \sum_{k=1}^{K} \sum_{g=1}^{G} x^r_{n,u,g} y_{n,i,g} l^2_{n,i,k,g} p^r_{n,k,g} \leq \epsilon_p \quad \forall n,i \tag{34b}$$

$$\sum_{n=1}^{N} \sum_{u=1}^{U_n} \sum_{g=1}^{G} x^r_{n,u,g} p^r_{n,k,g} T^{r-1}_n \leq E_k \quad \forall k \tag{34c}$$

$$\sum_{u=1}^{U_n} \sum_{g=1}^{G} x^r_{n,u,g} p^r_{n,k,g} \leq p_{max} \quad \forall n,k \tag{34d}$$

$$p^r_{n,k,g} \geq 0 \ v^r_{n,u,g} \geq 0 \quad \forall n,u,k,g \tag{34e}$$

where

$$\mathcal{D}_a(\mathbf{P}, \mathbf{T}, \mathbf{v}, \mathbf{x}) = \sum_{n=1}^{N} \sum_{u=1}^{U_n} \sum_{g=1}^{G} x_{n,u,g} T_n R_a(\mathbf{P}^r_{n,g}, v^r_{n,u,g}) \tag{35}$$

and

$$\begin{aligned} R_a(\mathbf{P}^r_{n,g}, v^r_{n,u,g}) &= \sum_{k=1}^{K} x_{n,u,g} T_n \log_2 \left(1 + \frac{M l^2_{n,u,k,g} p^r_{n,k,g}}{e^{v^r_{n,u,g}} \sigma^2}\right) \\ &+ x_{n,u,g} T_n M \log_2 e (v^r_{n,u,g} - 1 + e^{-v^r_{n,u,g}}). \end{aligned} \tag{36}$$

The equivalence between (18) and (34) can be proved by [31, Theorem 1]. Observing the formulation of (34), it can be further decomposed into two subproblems as

$$\max_{\mathbf{P}^j} \ \mathcal{D}_a(\mathbf{P}^j, \mathbf{T}^{r-1}, \mathbf{v}^{j-1}, \mathbf{x}^r) \tag{37a}$$

$$s.t. \quad \sum_{u=1}^{U_n} \sum_{k=1}^{K} \sum_{g=1}^{G} x^r_{n,u,g} y_{n,i,g} l^2_{n,i,k,g} p^j_{n,k,g} \leq \epsilon_p \quad \forall n,i \tag{37b}$$

$$\sum_{n=1}^{N} \sum_{u=1}^{U_n} \sum_{g=1}^{G} x^r_{n,u,g} p^j_{n,k,g} T^{r-1}_n \leq E_k \quad \forall k \tag{37c}$$

$$\sum_{u=1}^{U_n} \sum_{g=1}^{G} x^r_{n,u,g} p^j_{n,k,g} \leq p_{max} \quad \forall n,k \tag{37d}$$

$$p^j_{n,k,g} \geq 0 \quad \forall n,k,g \tag{37e}$$

and

$$\min_{\mathbf{v}^j} \ \mathcal{D}_a(\mathbf{P}^j, \mathbf{T}^{r-1}, \mathbf{v}^j, \mathbf{x}^r) \tag{38a}$$

Algorithm 2 Algorithm to solve (18)

Input: ϵ_p, $\{E_k, k = 1 \sim K\}$, p_{max}, $\mathbf{T}^{r-1}$, $\mathbf{x}^r$.

1: Initialization: $\epsilon_0 = 1 \times 10^{-3}$, $j = 1$, $\mathbf{P}^0 = \mathbf{0}$, $\mathbf{w}^0 = \mathbf{1}$;
2: Solve (32), denoting the optimal solution as $\mathbf{P}^*$, set $\mathbf{P}^1 = \mathbf{P}^*$;
3: **while** $|1 - \frac{\mathcal{D}_a(\mathbf{P}^{j-1}, \mathbf{T}^{r-1}, \mathbf{w}^{j-1}, \mathbf{x}^r)}{\mathcal{D}_a(\mathbf{P}^j, \mathbf{T}^{r-1}, \mathbf{w}^j, \mathbf{x}^r)}| > \epsilon_0$ **do**
4: Update $\mathbf{w}^j$ using (33);
5: $j = j + 1$;
6: Solve (32), denoting the optimal solution as $\mathbf{P}^*$, set $\mathbf{P}^j = \mathbf{P}^*$;

Output: $\mathbf{P}^j$, $\mathbf{w}^j$.

$$s.t. \ v^j_{n,u,g} \geq 0 \quad \forall n,u,g. \tag{38b}$$

Recalling the equivalence between (18) and (34), we can also conclude that (37) is equivalent to (32) and (38) is equivalent to (33). Thus, Algorithm 2 actually can find the solution to (34) in an iterative way. As $\mathcal{D}_a(\mathbf{P}, \mathbf{T}, \mathbf{v}, \mathbf{x})$ is convex with respect to $\mathbf{v}$ and concave with respect to $\mathbf{P}$, the convergence of Algorithm 2 is guaranteed based on the following theorem.

Theorem 1: Suppose

$$\begin{aligned} L(\mathbf{P}^r, \mathbf{v}^r, \boldsymbol{\nu}, \boldsymbol{\xi}, \boldsymbol{\theta}) &= \mathcal{D}_a(\mathbf{P}^r, \mathbf{T}^{r-1}, \mathbf{v}^r, \mathbf{x}^r) \\ &+ \sum_{n=1}^{N} \sum_{i=1}^{N_s} \nu_{n,i} (\epsilon_p - \sum_{u=1}^{U_n} \sum_{k=1}^{K} \sum_{g=1}^{G} x^r_{n,u,g} y_{n,i,g} l^2_{n,i,k,g} p^r_{n,k,g}) \\ &+ \sum_{k=1}^{K} \xi_k (E_k - \sum_{n=1}^{N} \sum_{u=1}^{U_n} \sum_{g=1}^{G} x^r_{n,u,g} p^r_{n,k,g} T^{r-1}_n) \\ &+ \sum_{n=1}^{N} \sum_{k=1}^{K} \theta_{n,k} (p_{max} - \sum_{u=1}^{U_n} \sum_{g=1}^{G} x^r_{n,u,g} p^r_{n,k,g}) \end{aligned} \tag{39}$$

is the Lagrangian dual function of (34) where $\boldsymbol{\nu}, \boldsymbol{\xi}, \boldsymbol{\theta}$ are Lagrangian multipliers, $\mathbf{P}^r$ and $\mathbf{v}^r$ satisfy (34e). Algorithm 2 will converge to the unique saddle point of $L(\mathbf{P}^r, \mathbf{v}^r, \boldsymbol{\nu}, \boldsymbol{\xi}, \boldsymbol{\theta})$ with respect to $\mathbf{P}^r$ and $\mathbf{v}^r$.

Proof: Firstly, we prove that the optimal solution to (34) is a unique saddle point of $L(\mathbf{P}^r, \mathbf{v}^r, \boldsymbol{\nu}, \boldsymbol{\xi}, \boldsymbol{\theta})$ with respect to $\mathbf{P}^r$ and $\mathbf{v}^r$. We know that $\mathcal{D}_a(\mathbf{P}^r, \mathbf{T}^{r-1}, \mathbf{v}^r, \mathbf{x}^r)$ is concave with respect to $\mathbf{P}^r$ and convex with respect to $\mathbf{v}^r$. Hence, it is not difficult to certificate that $L(\mathbf{P}^r, \mathbf{v}^r, \boldsymbol{\nu}, \boldsymbol{\xi}, \boldsymbol{\theta})$ is also concave with respect to $\mathbf{P}^r$ and convex with respect to $\mathbf{v}^r$, because (34b)–(34d) are linear constraints with respect to $\mathbf{P}^r$. As a result, the optimal solution to (34) is a unique saddle point of $L(\mathbf{P}^r, \mathbf{v}^r, \boldsymbol{\nu}, \boldsymbol{\xi}, \boldsymbol{\theta})$.

Actually, the purpose of Algorithm 2 is to find the optimal solution to (34) following the direction of subgradient at every step of the iteration. Hence, Algorithm 2 will naturally converge to the unique saddle point of $L(\mathbf{P}^r, \mathbf{v}^r, \boldsymbol{\nu}, \boldsymbol{\xi}, \boldsymbol{\theta})$. ■

Using the solutions to (17), (18) and (19), we propose an iterative algorithm to solve the optimization problem in (16). The steps of the proposed algorithm are summarized in Algorithm 3.

E. Convergence Analysis

In this section, the convergence of Algorithm 3 is analyzed. Actually, Algorithm 3 is guaranteed to converge. Denoting $\mathbf{x}^{r-1}$ as the solution to (17), $\mathbf{P}^{r-1}$ as the solution to (18) and $\mathbf{T}^{r-1}$ as the solutions to (19) at the $(r-1)$-th step. Firstly, at the r-th step of iteration, we have $\mathbf{x}^r$ after (17) is solved, which satisfies

$$\mathcal{D}_a(\mathbf{P}^{r-1},\mathbf{T}^{r-1},\mathbf{w}^{r-1},\mathbf{x}^r) \geq \mathcal{D}_a(\mathbf{P}^{r-1},\mathbf{T}^{r-1},\mathbf{w}^{r-1},\mathbf{x}^{r-1}). \tag{40}$$

The inequality in (40) is guaranteed due to the fact that $\mathbf{x}^r$ is derived using (25). In (25), both n and g are fixed when searching the maximum value of $V_{n,u,g}$ for varying u. According to (24), we can find that only $R_a(\mathbf{P}_{n,g}, w_{n,u,g})$ in $V_{n,u,g}$ is related to u. These two facts indicate that the operation in (25) can actually find the largest value of $R_a(\mathbf{P}_{n,g}, w_{n,u,g})$, or in other words, the value of $\mathcal{D}_a(\mathbf{P},\mathbf{T},\mathbf{w},\mathbf{x})$ is maximized.

Then, after (18) is solved, we have $\mathbf{P}^r$ as the optimal solution, and $\mathbf{w}^r$ can be calculated using (15), which satisfies

$$\mathcal{D}_a(\mathbf{P}^r,\mathbf{T}^{r-1},\mathbf{w}^r,\mathbf{x}^r) \geq \mathcal{D}_a(\mathbf{P}^{r-1},\mathbf{T}^{r-1},\mathbf{w}^{r-1},\mathbf{x}^r). \tag{41}$$

Finally, the optimal hovering time $\mathbf{T}^r$ is acquired by solving (19), which satisfies

$$\mathcal{D}_a(\mathbf{P}^r,\mathbf{T}^r,\mathbf{w}^r,\mathbf{x}^r) \geq \mathcal{D}_a(\mathbf{P}^r,\mathbf{T}^{r-1},\mathbf{w}^{r-1},\mathbf{x}^r). \tag{42}$$

Both (41) and (42) are guaranteed because $\mathcal{D}_a(\mathbf{P},\mathbf{T},\mathbf{w},\mathbf{x})$ is maximized in (18) and (19). Thus, we can conclude that

$$\mathcal{D}_a(\mathbf{P}^r,\mathbf{T}^r,\mathbf{w}^r,\mathbf{x}^r) \geq \mathcal{D}_a(\mathbf{P}^{r-1},\mathbf{T}^{r-1},\mathbf{w}^{r-1},\mathbf{x}^{r-1}) \tag{43}$$

which shows that the objective function of (16) keeps increasing at every step of the iteration, and it is upper bounded by the given resources. As a result, the convergence of Algorithm 3 is guaranteed, and at least a suboptimal solution is derived using this algorithm.

Remark 1: The subchannel allocation method in Section III.C implies that the UUs in better channel environment have more chance to be served by UAVs. Although the overall data transmission efficiency performance can be optimized by this strategy, the coverage ability of UAVs is hard to be guaranteed. More specifically, if a UU always stays in a bad channel environment for a long time, it can hardly be covered by UAVs. Such phenomenon inspires us to redesign the objective function of the original optimization problem.

IV. Process-oriented Minimum Data Transmission Efficiency Optimization

According to Remark 1, although the overall data transmission efficiency has been maximized in Section III, the coverage ability of the UAV swarm is hard to be guaranteed. In this section, we reformulate the original objective function to a max-min one, and then propose an algorithm to solve the coverage problem.

Algorithm 3 Proposed data transmission efficiency maximization algorithm

Input: ϵ_p, $\{E_k, k=1\sim K\}$, T_{total}, p_{max}, T_{max}.

1: Initialization: $\epsilon_0 = 1\times 10^{-2}$, $r=1$, $\mathbf{T}^0 = (T_{total}/N)\mathbf{1}$, $\mathbf{P}^0 = \mathbf{0}$;
2: Solve (17), denoting the solution as $\mathbf{x}^*$, set $\mathbf{x}^1 = \mathbf{x}^*$;
3: Solve (18), denoting the solution as $\mathbf{P}^*$, set $\mathbf{P}^1 = \mathbf{P}^*$;
4: Solve (19), denoting the solution as $\mathbf{T}^*$, set $\mathbf{T}^1 = \mathbf{T}^*$;
5: **while** $|1 - \frac{\mathcal{D}_a(\mathbf{P}^{r-1},\mathbf{T}^{r-1},\mathbf{w}^{r-1},\mathbf{x}^{r-1})}{\mathcal{D}_a(\mathbf{P}^r,\mathbf{T}^r,\mathbf{w}^r,\mathbf{x}^r)}| > \epsilon_0$ **do**
6: $r = r+1$;
7: Solve (17), denoting the solution as $\mathbf{x}^*$, set $\mathbf{x}^r = \mathbf{x}^*$;
8: Solve (18), denoting the solution as $\mathbf{P}^*$, set $\mathbf{P}^r = \mathbf{P}^*$;
9: Solve (19), denoting the solution as $\mathbf{T}^*$, set $\mathbf{T}^r = \mathbf{T}^*$;

Output: $\mathbf{x}^r$, $\mathbf{P}^r$, $\mathbf{T}^r$.

A. Problem Formulation and Decomposition

To improve the worst performance of all UUs, we can convert the original data transmission efficiency maximization problem (12) to a max-min optimization problem, where the minimum data transmission efficiency of UUs is maximized to guarantee the coverage ability. Further by using the transformation technique in Section III.A, the max-min optimization problem is reformulated as

$$\max_{\mathbf{P},\mathbf{T},\mathbf{x}} \ \min_{n,u} \ \sum_{g=1}^{G} x_{n,u,g} T_n R_a(\mathbf{P}_{n,g}, w_{n,u,g}) \tag{44a}$$

$$s.t. \ \sum_{u=1}^{U_n}\sum_{k=1}^{K}\sum_{g=1}^{G} x_{n,u,g} y_{n,i,g} l^2_{n,i,k,g} p_{n,k,g} \leq \epsilon_p \ \ \forall n,i \tag{44b}$$

$$\sum_{n=1}^{N}\sum_{u=1}^{U_n}\sum_{g=1}^{G} x_{n,u,g} p_{n,k,g} T_n \leq E_k \ \ \forall k \tag{44c}$$

$$\sum_{u=1}^{U_n}\sum_{g=1}^{G} x_{n,u,g} p_{n,k,g} \leq p_{max} \ \ \forall n,k \tag{44d}$$

$$\sum_{u=1}^{U_n} x_{n,u,g} \leq 1 \ \ \forall n,g \tag{44e}$$

$$\sum_{n=1}^{N} T_n \leq T_{total} \tag{44f}$$

$$T_n \leq T_{max} \ \ \forall n \tag{44g}$$

$$w_{n,u,g} = 1 + \sum_{k=1}^{K} \frac{l^2_{n,u,k,g} p_{n,k,g}}{\sigma^2 + M l^2_{n,u,k,g} p_{n,k,g} w^{-1}_{n,u,g}} \ \ \forall n,u,g \tag{44h}$$

$$x_{n,u,g} \in \{0,1\} \ p_{n,k,g} \geq 0 \ T_n \geq 0 \ \ \forall n,u,k,g. \tag{44i}$$

The objective function of (44) is the minimum data transmission efficiency of all UUs, and the practical constraints are derived in (44b)–(44i). As (44) is not convex and hard to be solved directly, we can decompose it into three subproblems. Denoting the iteration index as r, we can first formulate the

max-min subchannel allocation subproblem as

$$\max_{\mathbf{x}^r} \min_{n,u} \sum_{g=1}^{G} x^r_{n,u,g} T_n^{r-1} R_a(\mathbf{P}^{r-1}_{n,g}, w^{r-1}_{n,u,g}) \tag{45a}$$

$$s.t. \sum_{u=1}^{U_n}\sum_{k=1}^{K}\sum_{g=1}^{G} x^r_{n,u,g} y_{n,i,g} l^2_{n,i,k,g} p^{r-1}_{n,k,g} \le \epsilon_p \quad \forall n,i \tag{45b}$$

$$\sum_{n=1}^{N}\sum_{u=1}^{U_n}\sum_{g=1}^{G} x^r_{n,u,g} p^{r-1}_{n,k,g} T_n^{r-1} \le E_k \quad \forall k \tag{45c}$$

$$\sum_{u=1}^{U_n}\sum_{g=1}^{G} x^r_{n,u,g} p^{r-1}_{n,k,g} \le p_{max} \quad \forall n,k \tag{45d}$$

$$\sum_{u=1}^{U_n} x^r_{n,u,g} \le 1 \quad \forall n,g \tag{45e}$$

$$x^r_{n,u,g} \in \{0,1\} \quad \forall n,u,g. \tag{45f}$$

Then, we can derive the max-min power allocation subproblem as

$$\max_{\mathbf{P}^r} \min_{n,u} \sum_{g=1}^{G} x^r_{n,u,g} T_n^{r-1} R_a(\mathbf{P}^{r}_{n,g}, w^{r}_{n,u,g}) \tag{46a}$$

$$s.t. \sum_{u=1}^{U_n}\sum_{k=1}^{K}\sum_{g=1}^{G} x^r_{n,u,g} y_{n,i,g} l^2_{n,i,k,g} p^{r}_{n,k,g} \le \epsilon_p \quad \forall n,i \tag{46b}$$

$$\sum_{n=1}^{N}\sum_{u=1}^{U_n}\sum_{g=1}^{G} x^r_{n,u,g} p^{r}_{n,k,g} T_n^{r-1} \le E_k \quad \forall k \tag{46c}$$

$$\sum_{u=1}^{U_n}\sum_{g=1}^{G} x^r_{n,u,g} p^{r}_{n,k,g} \le p_{max} \quad \forall n,k \tag{46d}$$

$$w^r_{n,u,g} = 1 + \sum_{k=1}^{K} \frac{l^2_{n,u,k,g} p^r_{n,k,g}}{\sigma^2 + M l^2_{n,u,k,g} p^r_{n,k,g} (w^r_{n,u,g})^{-1}} \quad \forall n,u,g \tag{46e}$$

$$p^r_{n,k,g} \ge 0 \quad \forall n,k,g \tag{46f}$$

and we can derive the max-min hovering time scheduling subproblem as

$$\max_{\mathbf{T}^r} \min_{n,u} \sum_{g=1}^{G} x^r_{n,u,g} T^r_n R_a(\mathbf{P}^{r}_{n,g}, w^{r}_{n,u,g}) \tag{47a}$$

$$s.t. \sum_{n=1}^{N}\sum_{u=1}^{U_n}\sum_{g=1}^{G} x^r_{n,u,g} p^r_{n,k,g} T^r_n \le E_k \quad \forall k \tag{47b}$$

$$\sum_{n=1}^{N} T^r_n \le T_{total} \tag{47c}$$

$$0 \le T^r_n \le T_{max} \quad \forall n. \tag{47d}$$

Observing the formulations of three subproblems, we can find that (47) is a linear max-min optimization problem, which can be directly solved using conventional max-min optimization tools [36]. Hence, we focus on giving the solutions to (45) and (46).

B. Max-min Subchannel Allocation

To solve (45), we define a slack variable τ, which satisfies

$$\tau = \min_{n,u} \sum_{g=1}^{G} x^r_{n,u,g} T_n^{r-1} R_a(\mathbf{P}^{r-1}_{n,g}, w^{r-1}_{n,u,g}). \tag{48}$$

Using (48), (45) can be equivalently transformed to

$$\max_{\mathbf{x}^r,\tau} \tau \tag{49a}$$

$$s.t. \sum_{g=1}^{G} x^r_{n,u,g} T_n^{r-1} R_a(\mathbf{P}^{r-1}_{n,g}, w^{r-1}_{n,u,g}) \ge \tau \quad \forall n,u \tag{49b}$$

$$\sum_{u=1}^{U_n}\sum_{k=1}^{K}\sum_{g=1}^{G} x^r_{n,u,g} y_{n,i,g} l^2_{n,i,k,g} p^{r-1}_{n,k,g} \le \epsilon_p \quad \forall n,i \tag{49c}$$

$$\sum_{n=1}^{N}\sum_{u=1}^{U_n}\sum_{g=1}^{G} x^r_{n,u,g} p^{r-1}_{n,k,g} T_n^{r-1} \le E_k \quad \forall k \tag{49d}$$

$$\sum_{u=1}^{U_n}\sum_{g=1}^{G} x^r_{n,u,g} p^{r-1}_{n,k,g} \le p_{max} \quad \forall n,k \tag{49e}$$

$$\sum_{u=1}^{U_n} x^r_{n,u,g} \le 1 \quad \forall n,g \tag{49f}$$

$$x^r_{n,u,g} \in \{0,1\} \quad \forall n,u,g. \tag{49g}$$

We can observe that (49) is an ILP problem and hard to be solved directly. Actually, (49) can be simplified according to the following theorem.

Theorem 2: Relaxing the constraints in (49c)–(49e) will not change the optimal solution to (49).

Proof: See Appendix A. ■

Theorem 2 indicates that the constraint of the minimum data transmission efficiency has the highest priority compared with other practical constraints, due to the fact that it is a transformed form of the objective function. According to Theorem 2, we can equivalently derive a simplified formulation of (49) as

$$\max_{\mathbf{x}^r,\tau} \tau \tag{50a}$$

$$s.t. \sum_{g=1}^{G} x^r_{n,u,g} T_n^{r-1} R_a(\mathbf{P}^{r-1}_{n,g}, w^{r-1}_{n,u,g}) \ge \tau \quad \forall n,u \tag{50b}$$

$$\sum_{u=1}^{U_n} x^r_{n,u,g} \le 1 \quad \forall n,g \tag{50c}$$

$$x^r_{n,u,g} \in \{0,1\} \quad \forall n,u,g. \tag{50d}$$

To solve (50), we have a property which can give the condition that the solution to (50) must satisfy, which is

Property 1: Suppose that $\mathbf{x}^{r*}$ is a non-trivial solution to (50), $\mathbf{x}^{r*}$ must satisfy

$$\sum_{g=1}^{G} x^r_{n,u,g} \ge 1 \quad \forall n,u. \tag{51}$$

Otherwise, if (51) is not satisfied, (50) only has a trivial solution, which means the maximum value of τ is 0.

Algorithm 4 Max-min subchannel allocation algorithm

Input: $\mathbf{T}^{r-1}$, $\mathbf{P}^{r-1}$, $\mathbf{w}^{r-1}$;

Initialization: $\epsilon_0 = 1 \times 10^{-3}$, $j = 1$, $\tau^0 = 0$;
Initialize $\mathbf{x}^1$ according to [37];
Define $V_{n,u}^j = \sum_{g=1}^{G} x_{n,u,g}^j T_n^{r-1} R_a(\mathbf{P}_{n,g}^{r-1}, w_{n,u,g}^{r-1})$;
Set $\tau^j = \min_{n,u} V_{n,u}^j$;
while $|1 - \frac{\tau^{j-1}}{\tau^j}| > \epsilon_0$ **do**
  for n = 1:N **do**
    Find the minimum value of $V_{n,u}^j$, denoting the index as u^*;
    Find the maximum value of $V_{n,u}^j$ that satisfies the condition $\sum_{g=1}^{G} x_{n,u,g}^j > 1$, denoting the index as u^{**};
    Define the index set as $I = \{g | x_{n,u^{**},g}^j = 1\}$;
    Find $g^* = \arg\min_{g \in I} T_n^{r-1} R_a(\mathbf{P}_{n,g}^{r-1}, w_{n,u^{**},g}^{r-1})$;
    if $V_{n,u^*}^j + T_n^{r-1} R_a(\mathbf{P}_{n,g^*}^{r-1}, w_{n,u^*,g^*}^{r-1}) \leq V_{n,u^{**}}^j - T_n^{r-1} R_a(\mathbf{P}_{n,g^*}^{r-1}, w_{n,u^{**},g^*}^{r-1})$ **then**
      Set $x_{n,u^*,g^*}^j = 1$;
      Set $x_{n,u^{**},g^*}^j = 0$;
  $j = j + 1$;
  Set $\tau^j = \min_{n,u} V_{n,u}^j$;

Output: $\mathbf{x}^j$.

Proof: If (51) is not satisfied, as the components in $\mathbf{x}^r$ are discrete variables, there exists $n^* \in \{1, ..., N\}$ and $u^* \in \{1, ..., U_n^*\}$ which satisfy

$$\sum_{g=1}^{G} x_{n^*,u^*,g}^r = 0 \tag{52}$$

which means $x_{n^*,u^*,g}^r$ is 0 for all $g \in \{1, ..., G\}$. Substituting $x_{n^*,u^*,g}^r$ into (50), we can find that the maximum value of τ is 0. Hence, the conclusion of Property 1 is given. ■

Using Property 1 and Theorem 2, a solution to (45) can be derived based on (50) in a greedy manner, which is summarized in Algorithm 4. At every step of Algorithm 4, the minimum data transmission efficiency is improved by allocating the subchannel to the user in worst condition. Hence, Algorithm 4 can converge to the suboptimal solution to (45).

Remark 2: It is worth noting that we have used two different methods to solve the subchannel allocation subproblem in Section III.C and the max-min subchannel allocation subproblem in Section IV.B. The reason is that the algorithms are designed to accommodate the objective functions of different problems, in order to achieve better performance. The variable recovery algorithm in Section III.C can optimize the overall data transmission efficiency, while the method in Section IV.B can improve the minimum data transmission efficiency.

C. Max-min Power Allocation

In this section, we propose an algorithm to solve (46). Similar with (49), we introduce the slack variable τ and reformulate (46) as

$$\max_{\mathbf{P}^r, \tau} \ \tau \tag{53a}$$

$$s.t. \quad \sum_{g=1}^{G} x_{n,u,g}^r T_n^{r-1} R_a(\mathbf{P}_{n,g}^r, w_{n,u,g}^r) \geq \tau \quad \forall n, u \tag{53b}$$

$$\sum_{u=1}^{U_n} \sum_{k=1}^{K} \sum_{g=1}^{G} x_{n,u,g}^r y_{n,i,g} l_{n,i,k,g}^2 p_{n,k,g}^r \leq \epsilon_p \quad \forall n, i \tag{53c}$$

$$\sum_{n=1}^{N} \sum_{u=1}^{U_n} \sum_{g=1}^{G} x_{n,u,g}^r p_{n,k,g}^r T_n^{r-1} \leq E_k \quad \forall k \tag{53d}$$

$$\sum_{u=1}^{U_n} \sum_{g=1}^{G} x_{n,u,g}^r p_{n,k,g}^r \leq p_{max} \quad \forall n, k \tag{53e}$$

$$w_{n,u,g}^r = 1 + \sum_{k=1}^{K} \frac{l_{n,u,k,g}^2 p_{n,k,g}^r}{\sigma^2 + M l_{n,u,k,g}^2 p_{n,k,g}^r (w_{n,u,g}^r)^{-1}} \quad \forall n, u, g \tag{53f}$$

$$p_{n,u,k,g}^r \geq 0 \quad \forall n, u, k, g. \tag{53g}$$

Note that (53) is not convex, due to the coupling between $\mathbf{P}$ and $\mathbf{w}$ in (53b) and (53f). To cope with this challenge, we can transform (53b) and relax (53f) based on the following theorem.

Theorem 3: The constraints (53b) and (53f) can be equivalently transformed to

$$\sum_{g=1}^{G} x_{n,u,g}^r T_n^{r-1} R_a(\mathbf{P}_{n,g}^r, v_{n,u,g}^r) \geq \tau \quad \forall n, u$$
$$v_{n,u,g}^r \geq 0 \quad \forall n, u, g \tag{54}$$

where $R_a(\mathbf{P}_{n,g}^r, v_{n,u,g}^r)$ has been defined in (36).

Proof: See Appendix B. ■

Theorem 3 indicates that (53b) and (53f) can be replaced by (54), which means $\mathbf{P}^r$ and $\mathbf{v}^r$ are decoupled. Consequently, (53) can be solved using conventional successive convex optimization method, but the computational overhead is too large for UAVs to serve massive users [38]. Hence, we propose an iterative algorithm to reduce the complexity, after (53) is reformulated as

$$\max_{\mathbf{P}^j, \tau^j} \ \tau^j \tag{55a}$$

$$s.t. \quad \sum_{g=1}^{G} x_{n,u,g}^r T_n^{r-1} R_a(\mathbf{P}_{n,g}^j, v_{n,u,g}^{j-1}) \geq \tau^j \quad \forall n, u \tag{55b}$$

$$\sum_{u=1}^{U_n} \sum_{k=1}^{K} \sum_{g=1}^{G} x_{n,u,g}^r y_{n,i,g} l_{n,i,k,g}^2 p_{n,k,g}^j \leq \epsilon_p \quad \forall n, i \tag{55c}$$

$$\sum_{n=1}^{N} \sum_{u=1}^{U_n} \sum_{g=1}^{G} x_{n,u,g}^r p_{n,k,g}^j T_n^{r-1} \leq E_k \quad \forall k \tag{55d}$$

$$\sum_{u=1}^{U_n} \sum_{g=1}^{G} x_{n,u,g}^r p_{n,k,g}^j \leq p_{max} \quad \forall n, k \tag{55e}$$

$$p_{n,u,k,g}^j \geq 0 \quad \forall n, u, k, g. \tag{55f}$$

Algorithm 5 Algorithm to solve (53)

Input: ϵ_p, $\{E_k, k = 1 \sim K\}$, p_{max}.

1: Initialization: $\epsilon_0 = 1 \times 10^{-3}$, $j = 1$, $\mathbf{P}^0 = \mathbf{0}$, $\mathbf{v}^0 = \mathbf{0}$, $\tau^0 = 0$;
2: Solve (55), denoting the optimal solution as $(\mathbf{P}^*, \tau^*)$, set $\mathbf{P}^1 = \mathbf{P}^*$, $\tau^1 = \tau^*$;
3: **while** $|1 - \frac{\tau^{j-1}}{\tau^j}| > \epsilon_0$ **do**
4: $j = j + 1$;
5: Update $\mathbf{v}^{j-1}$ using (56);
6: Solve (55), denoting the optimal solution as $(\mathbf{P}^*, \tau^*)$, set $\mathbf{P}^j = \mathbf{P}^*$, $\tau^j = \tau^*$;

Output: $\mathbf{P}^j$, τ^j.

where the iteration index is j. In (55), $\mathbf{v}^{j-1}$ is regarded as a constant at the j-th step of iteration, and it is updated at the $(j-1)$-th step by solving the following equation

$$e^{v_{n,u,g}^{j-1}} = 1 + \sum_{k=1}^{K} \frac{l_{n,u,k,g}^2 p_{n,k,g}^{j-1}}{\sigma_m^2 + M l_{n,u,k,g}^2 p_{n,k,g}^{j-1} e^{-v_{n,u,g}^{j-1}}}. \quad (56)$$

It is worth noting that (55) is convex, so that it can be readily solved using conventional convex optimization tools. The proposed iterative algorithm is summarized in Algorithm 5. To prove the convergence of Algorithm 5, we can derive the Lagrangian function of (55) as

$$\begin{aligned} &L(\mathbf{P}^j, \mathbf{v}^{j-1}, \tau^j, \boldsymbol{\psi}, \boldsymbol{\nu}, \boldsymbol{\xi}, \boldsymbol{\theta}) = \tau^j \\ &+ \sum_{n=1}^{N} \sum_{u=1}^{U_n} \psi_{n,u} \Big(\sum_{g=1}^{G} x_{n,u,g}^r T_n^{r-1} R_a(\mathbf{P}_{n,g}^j, v_{n,u,g}^{j-1}) - \tau^j \Big) \\ &+ \sum_{n=1}^{N} \sum_{i=1}^{N_s} \nu_{n,i} \Big(\epsilon_p - \sum_{u=1}^{U_n} \sum_{k=1}^{K} \sum_{g=1}^{G} x_{n,u,g}^r y_{n,i,g} l_{n,i,k,g}^2 p_{n,k,g}^j \Big) \\ &+ \sum_{k=1}^{K} \xi_k \Big(E_k - \sum_{n=1}^{N} \sum_{u=1}^{U_n} \sum_{g=1}^{G} x_{n,u,g}^r p_{n,k,g}^j T_n^{r-1} \Big) \\ &+ \sum_{n=1}^{N} \sum_{k=1}^{K} \theta_{n,k} \Big(p_{max} - \sum_{u=1}^{U_n} \sum_{g=1}^{G} x_{n,u,g}^r p_{n,k,g}^j \Big) \end{aligned} \quad (57)$$

Actually, the purpose of Algorithm 5 is to find the unique saddle point of (57), due to the fact that (57) is concave with respect to $\mathbf{P}^j$ and convex with respect to $\mathbf{v}^{j-1}$. According to Theorem 1, Algorithm 5 is guaranteed to converge.

In summary, (44) can be iteratively solved based on the solutions to (45)–(47). We record the steps of this method in Algorithm 6. Similar with Algorithm 3, the convergence of Algorithm 6 is naturally guaranteed, and at least a suboptimal solution is derived.

Remark 3: Observing the methods proposed in Section III and IV, we can find some similarities and differences. One one hand, both optimization problems are solved in an iterative way, because both of them focus on jointly allocating the subchannel, transmit power and hovering time. On the other hand, the max-min subchannel allocation subproblem in IV.B can not be solved based on the time-sharing relaxation, because the worst performance of all users will be affected by the relaxation technique. Besides, a series of transformation steps is required to solve the max-min power allocation subproblem in IV.C, due to the fact that the new objective function is more complicated than the original one.

Algorithm 6 Proposed minimum data transmission efficiency optimization algorithm

Input: ϵ_p, $\{E_k, k = 1 \sim K\}$, T_{total}, p_{max}, T_{max}.

1: Initialization:$\epsilon_0 = 1 \times 10^{-2}$, $r = 1$, $\mathbf{T}^0 = (T_{total}/N)\mathbf{1}$, $\mathbf{P}^0 = \mathbf{0}$;
2: Solve (45), denoting the solution as $\mathbf{x}^*$, set $\mathbf{x}^1 = \mathbf{x}^*$;
3: Solve (46), denoting the solution as $\mathbf{P}^*$, set $\mathbf{P}^1 = \mathbf{P}^*$;
4: Solve (47), denoting the solution as $\mathbf{T}^*$, set $\mathbf{T}^1 = \mathbf{T}^*$;
5: **while** $|1 - \frac{\min_{n,u} \sum_{g=1}^{G} x_{n,u,g}^{r-1} T_n^{r-1} R_a(\mathbf{P}_{n,u,g}^{r-1}, w_{n,u,g}^{r-1})}{\min_{n,u} \sum_{g=1}^{G} x_{n,u,g}^{r} T_n^{r} R_a(\mathbf{P}_{n,u,g}^{r}, w_{n,u,g}^{r})}| > \epsilon_0$ **do**
6: $r = r + 1$;
7: Solve (45), denoting the solution as $\mathbf{x}^*$, set $\mathbf{x}^r = \mathbf{x}^*$;
8: Solve (46), denoting the solution as $\mathbf{P}^*$, set $\mathbf{P}^r = \mathbf{P}^*$;
9: Solve (47), denoting the solution as $\mathbf{T}^*$, set $\mathbf{T}^r = \mathbf{T}^*$;

Output: $\mathbf{x}^r$, $\mathbf{P}^r$, $\mathbf{T}^r$.

V. Simulation Results and Discussions

In this section, we present simulation results to evaluate the proposed algorithms. Specifically, we fix the number of UAVs in a swarm at $K = 6$, the number of user group at $N = 20$, and the number of SU at $N_s = 10$. In each user group, we assume the number of UU is $U_n = 10$ for $\forall n$, so that the total number of UU is $N_U = 200$, and each UU is equipped with $M = 6$ antennas. Besides, we consider a broadband system which works at 5.8 GHz with $G = 16$ subchannels.[1] For the UAV channel, we generate the large-scale CSI based on the realistic channel environment [25], [26] using a simulation software named as Visualyze 7. The locations of UAVs, UUs and SUs, as well as the subchannel usage of SUs, are sample data generated by this software, and the noise power is set at $\sigma^2 = -107$ dBm. We set the interference power threshold at -77 dBm and the power limit of a UAV at $p_{max} = 300$ mW. The total hovering time of UAVs is set at $T_{total} = 100$ s, and the maximum hovering time of the UAV swarm at each UU is set at $T_{max} = 15$ s for more flexible time scheduling. For simplicity, we assume that each UAV has the same E_k for $\forall k$, and the sum of E_k is denoted as E_{total}.

Firstly, we analyze the complexity of the proposed algorithms through simulations. Specifically, we focus on the convergence performance of the proposed algorithms. In Fig. 2, the iteration times of 10 trials with different user locations are evaluated, where $E_{total} = 30$ J. For Algorithm 3, it only needs 2 iterations to converge. The reason for this phenomenon is that the best subchannel is selected by this algorithm at the first iteration, and the problem is almost convex with respect to the transmit power and hovering time when the subchannel usage is determined. For Algorithm 6, the number of iterations

[1] In practice, more users can be served by using the proposed scheme, because there are actually more available subchannels. For example, if the bandwidth is 20 MHz and the subcarrier spacing is 15 kHz, there are at least 1200 available subchannels. In this case, over 15000 users can be served.

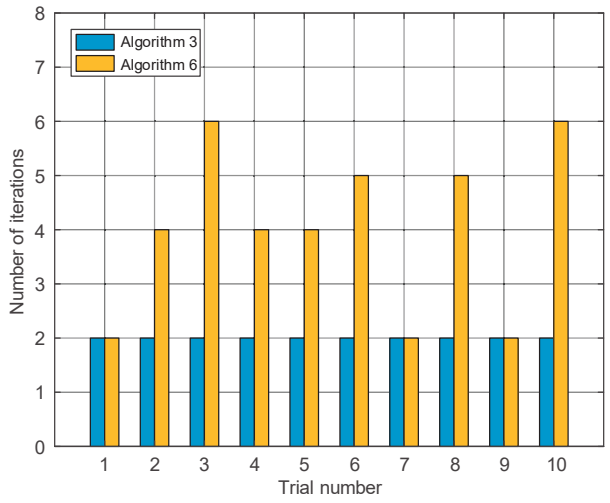

Fig. 2. Convergence performance of the proposed algorithms.

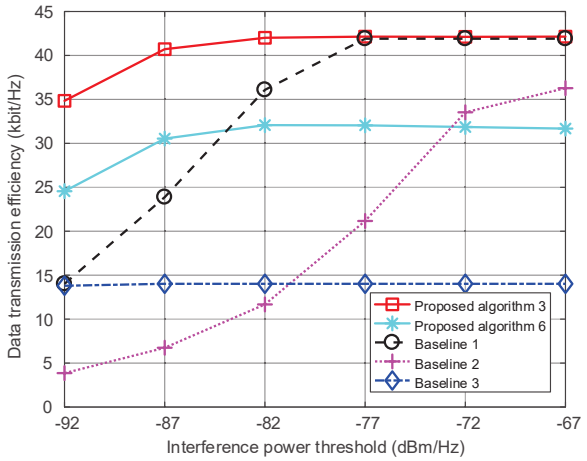

Fig. 3. Comparison of different algorithms considering the total data transmission efficiency.

is no more than 6, and the average number of it is 4 over 10 trials. These results demonstrate that the convergence speed of the proposed algorithms is fast, which also indicates that the algorithms have good potential in being applied to CSUNs in practice.

Then, we compare the performances of the proposed algorithms with other algorithms. For other algorithms, the subchannel allocation strategy, the power allocation strategy and the hovering time scheduling method are separately optimized. More specifically, the proposed algorithms are compared with the following baselines:

- *Baseline 1:* Allocating the subchannels based on path loss using the technique in [37] under conventional cellular architecture, then using the power allocation algorithm and hovering time scheduling algorithm in [21].
- *Baseline 2:* Allocating the subchannels based on path loss using the technique in [37] under conventional cellular architecture, then using the power allocation algorithm and hovering time scheduling algorithm in [23].
- *Baseline 3:* Allocating the subchannels based on path loss using the technique in [37] under conventional cellular architecture, then equally allocating the transmit power and hovering time.

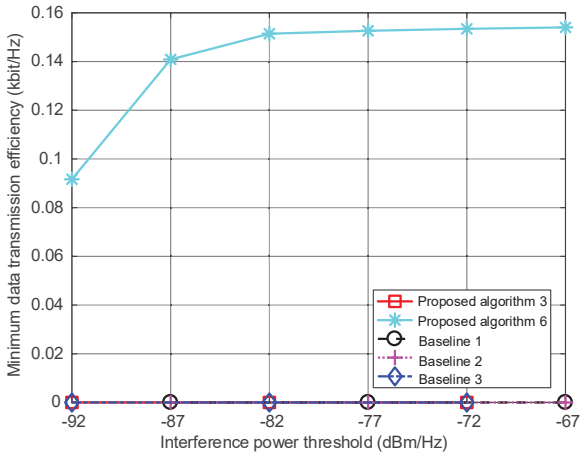

Fig. 4. Comparison of different algorithms regarding the minimum data transmission efficiency.

Besides, for the algorithms without interference constraints, the transmit power is divided by a large constant, so that the interference power constraints can be satisfied.

In Fig. 3, we evaluate the performances of different algorithms in terms of the data transmission efficiency for different interference power thresholds, where $E_{total} = 30$ J. We can observe that the proposed Algorithm 3 has the best performance when the interference power threshold is low. When the interference power threshold increases, Baseline 1 approaches Algorithm 3. The reason is that the interference constraint was not considered by the algorithm in [21], but such constraint will be negligible when the interference power threshold is high. Moreover, we can find that Baseline 2, where the algorithm in [23] ignored the effect of large-scale CSI, performs worse than the equal power allocation strategy with low interference power threshold. This indicates that the inaccurate estimation of the interference can seriously affect the performance of CSUNs.

We further discuss the minimum data transmission efficiency of different algorithms in Fig. 4. From the curves, we can observe that the minimum data transmission efficiency cannot be guaranteed by conventional algorithms, because the subchannels would not be allocated to UUs in severe channel environment. Such strategy can effectively maximize the total data transmission efficiency of all UUs. This figure also demonstrates that the proposed Algorithm 6 can effectively improve the minimum data transmission efficiency. Besides, as shown in Fig. 3 and Fig. 4, the total data transmission efficiency is actually to some extent guaranteed by the proposed Algorithm 6 when the minimum data transmission efficiency is optimized.

In Fig. 5, we demonstrate how the coverage ability of CSUN is optimized by Algorithm 6. To make the figure clearer, we discuss a simplified CSUN model, where 4 UUs are covered at one time slot, the interference power threshold is set at -92 dBm, and $E_{total} = 30$ J. When the user can receive the signal whose power is larger than -92 dBm, we regard this user as a successfully covered one. Following this, we can acquire

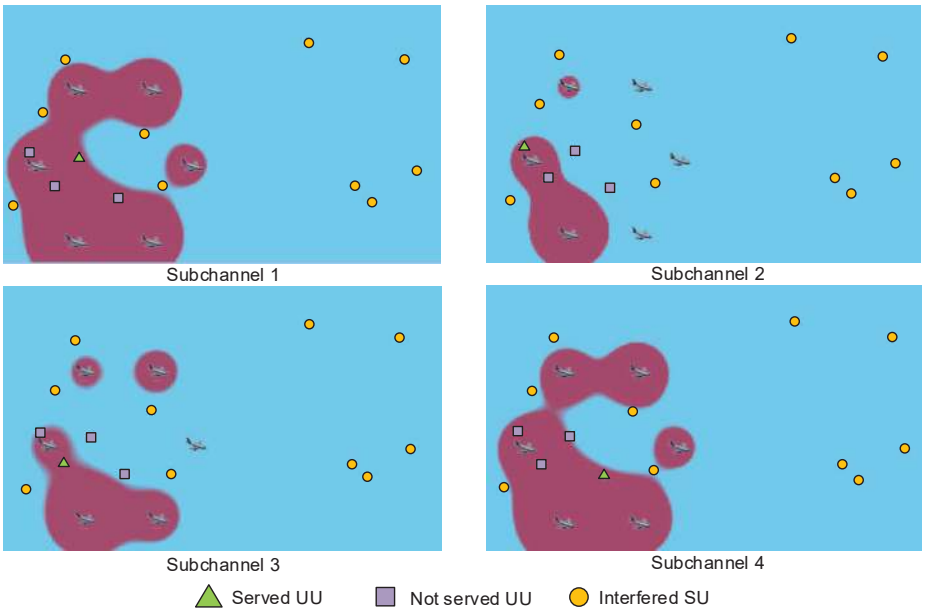

Fig. 5. Diagram of CSUN under non-cellular architecture, where the coverage areas at one time slot are plotted.

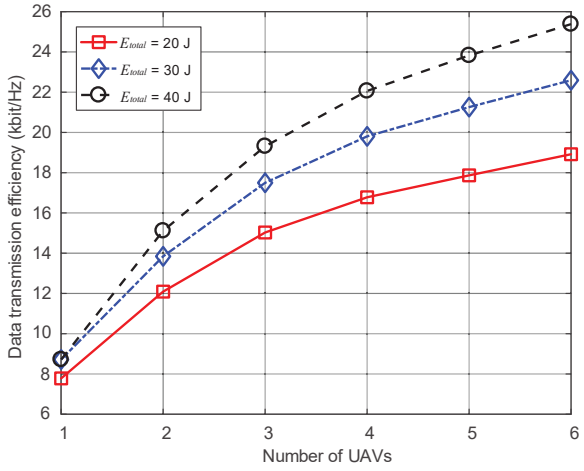

Fig. 6. The relationship between the total data transmission efficiency and the number of UAVs, where the proposed Algorithm 3 is used.

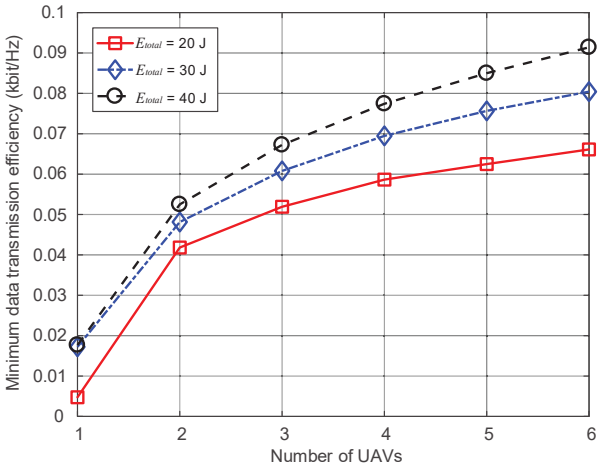

Fig. 7. The relationship between the minimum data transmission efficiency and the number of UAVs, where the proposed Algorithm 6 is used.

the coverage areas when different subchannels are used. As shown in Fig. 5, the users in plotted regions are actually covered. We can observe that the shapes of the coverage areas are irregular, indicating that the broadband CSUN is designed under non-cellular architecture. The result shows that Algorithm 6 can effectively mitigate the interference while guaranteeing the coverage ability of CSUN, which also implies the superiority of the non-cellular architecture over conventional cellular architectures.

Moreover, we concentrate on analyzing the relationship between the size of UAV swarm and the performances of proposed algorithms in Fig. 6 and Fig. 7. As shown by the curves, both the total data transmission efficiency and the minimum data transmission efficiency can be improved by increasing the number of UAVs. One reason is that a higher diversity gain can be obtained with more UAVs in a swarm. Moreover, the coordination among multiple UAVs is more flexible when the size of UAV swarm is larger. We can also observe that a better performance is achieved by both algorithms with higher transmit energy. These results imply that the limited on-board energy of the UAV swarm is a bottleneck of CSUNs.

In Fig. 8 and Fig. 9, the relationship between the number of subchannels and the performances of the proposed algorithms is evaluated. We can observe that better performance is achieved when more subchannels are adopted for both algorithms. Note that the curves in Fig. 9 demonstrate that the performance gain when improving the communication energy is not stable for different number of subchannels. This phenomenon emerges because a suboptimal solution is derived by using Algorithm 6, which implies that the number of subchannels should be appropriately selected for more efficient use of resources in broadband CSUNs.

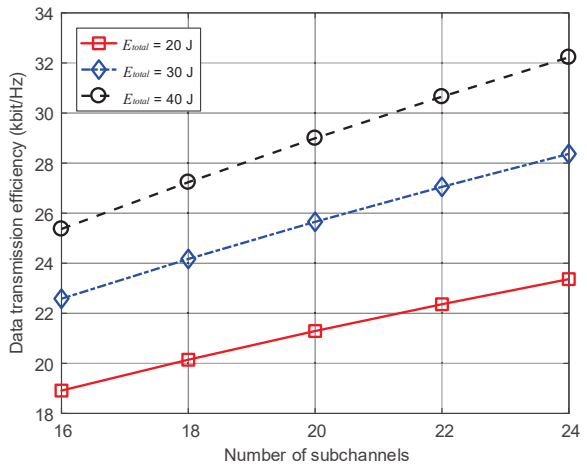

Fig. 8. The relationship between the total data transmission efficiency and the number of subchannels, where the proposed Algorithm 3 is used.

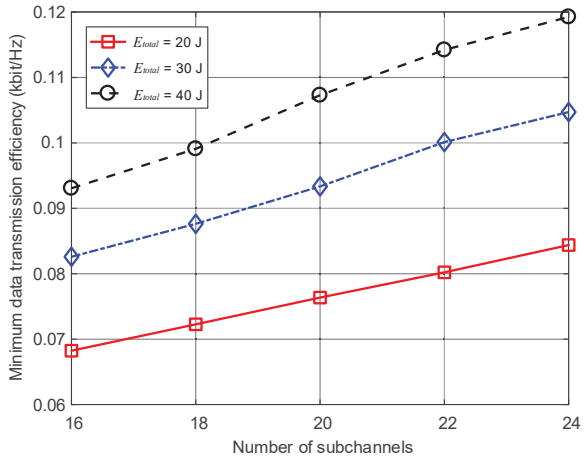

Fig. 9. The relationship between the minimum data transmission efficiency and the number of subchannels, where the proposed Algorithm 6 is used.

VI. Conclusion

In this paper, we have investigated the design of broadband CSUNs under non-cellular architecture, to serve massive IoT devices in wide areas. We have proposed a process-oriented optimization framework, where the flight process of UAVs was optimized based on slowly-varying CSI in a large time scale. We have formulated a data transmission efficiency maximization problem and a minimum data transmission efficiency optimization problem based on the process-oriented model. After the optimization problems have been solved using the time-sharing relaxation and feasible region relaxation techniques, the subchannel usage, transmit power and hovering time of the broadband CSUN are jointly optimized in an iterative way. Simulation results have demonstrated that it is beneficial to use the proposed algorithms when designing CSUNs for massive IoT devices under non-cellular architecture.

Appendix A
Proof of Theorem 2

To prove Theorem 2, we need to prove that for any $\mathbf{x}$ that satisfies (49b), (49f) and (49g), (49c)–(49e) are also satisfied. Assuming that we have obtained the optimal $\mathbf{P}^{r-1}$ and $\mathbf{x}^{r-1}$ at the $(r-1)$-th step. If $\mathbf{x}$ is an all-zero vector, the constraints are naturally satisfied. Otherwise, for any non-zero $\mathbf{x}$ which satisfies (49b), (49f) and (49g), and for any given $n^* \in \{1,...,N\}$, $g^* \in \{1,...,G\}$ and $k^* \in \{1,...,K\}$, we have

$$\sum_{u=1}^{U_{n^*}} x_{n^*,u,g^*} p_{n^*,k^*,g^*}^{r-1} = \sum_{u=1}^{U_{n^*}} x_{n^*,u,g^*}^{r-1} p_{n^*,k^*,g^*}^{r-1} \tag{A.1}$$

because only one of x_{n^*,u,g^*}^{r-1} for $u \in \{1,...,U_{n^*}\}$ equals to 1, which is also correct for $\mathbf{x}$, according to (49f) and (49g). Hence, based on (A.1), we have

$$\begin{aligned}&\sum_{u=1}^{U_n}\sum_{k=1}^{K}\sum_{g=1}^{G} x_{n,u,g} p_{n,k,g}^{r-1} y_{n,i,g} l_{n,i,k,g}^2 \\ &= \sum_{u=1}^{U_n}\sum_{k=1}^{K}\sum_{g=1}^{G} x_{n,u,g}^{r-1} p_{n,k,g}^{r-1} y_{n,i,g} l_{n,i,k,g}^2 \\ &\le \epsilon_p \quad \forall n,i\end{aligned} \tag{A.2}$$

$$\begin{aligned}&\sum_{u=1}^{U_n}\sum_{n=1}^{N}\sum_{g=1}^{G} x_{n,u,g} p_{n,k,g}^{r-1} T_n^{r-1} \\ &= \sum_{u=1}^{U_n}\sum_{n=1}^{N}\sum_{g=1}^{G} x_{n,u,g}^{r-1} p_{n,k,g}^{r-1} T_n^{r-1} \le E_k \quad \forall k\end{aligned} \tag{A.3}$$

$$\begin{aligned}&\sum_{u=1}^{U_n}\sum_{g=1}^{G} x_{n,u,g} p_{n,k,g}^{r-1} \\ &= \sum_{u=1}^{U_n}\sum_{g=1}^{G} x_{n,u,g}^{r-1} p_{n,k,g}^{r-1} \le p_{max} \quad \forall n,k.\end{aligned} \tag{A.4}$$

As a result, we can conclude that for any $\mathbf{x}$ that satisfies (49b), (49f) and (49g), (49c)–(49e) are also satisfied, which gives the conclusion of Theorem 2.

Appendix B
Proof of Theorem 3

We firstly define $v_{n,u,g}^r = \log(w_{n,u,g}^r)$ and substitute $\mathbf{v}^r$ into (53b) and (53f), then we have

$$\sum_{g=1}^{G} x_{n,u,g}^r T_n^{r-1} R_a(\mathbf{P}_{n,g}^r, v_{n,u,g}^r) \ge \tau \tag{B.1}$$

$$e^{v_{n,u,g}^r} = 1 + \sum_{k=1}^{K} \frac{l_{n,u,k,g}^2 p_{n,k,g}^r}{\sigma^2 + M l_{n,u,k,g}^2 p_{n,k,g}^r e^{-v_{n,u,g}^r}} \quad \forall n,u,g. \tag{B.2}$$

According to [21], if $\mathbf{v}^{r*}$ satisfies (B.2), we have

$$R_a(\mathbf{P}_{n,g}^r, v_{n,u,g}^r) \ge R_a(\mathbf{P}_{n,g}^r, v_{n,u,g}^{r*}) \quad \forall v_{n,u,g}^r \ge 0 \tag{B.3}$$

due to the fact that the minimum value of $R_a(\mathbf{P}_{n,g}^r, v_{n,u,g}^r)$ is achieved by $R_a(\mathbf{P}_{n,g}^r, v_{n,u,g}^{r*})$. Hence, we have

$$\sum_{g=1}^{G} x_{n,u,g}^r T_n^{r-1} R_a(\mathbf{P}_{n,g}^r, v_{n,u,g}^r) \ge \tau \quad \forall v_{n,u,g}^r \ge 0. \tag{B.4}$$

On the contrary, if (B.4) is satisfied, we can also have (B.1) and (B.2), because (B.4) is a more general condition, which is also correct for the $\mathbf{v}^{r*}$ in special cases. Hence, (B.1) and (B.2) can be replaced by (B.4), which gives the conclusion of Theorem 3.

REFERENCES

[1] R. Jia, X. Chen, Q. Qi and H. Lin, "Massive beam-division multiple access for B5G cellular Internet of Things," *IEEE Internet Things J.*, vol. 7, no. 3, pp. 2386-2396, Mar. 2020, doi: 10.1109/JIOT.2019.2958129.

[2] Q. Qi, X. Chen and D. W. K. Ng, "Robust beamforming for NOMA-based cellular massive IoT with SWIPT," *IEEE Trans. Signal Process.*, vol. 68, pp. 211-224, 2020, doi: 10.1109/TSP.2019.2959246.

[3] A. Ikpehai et al., "Low-power wide area network technologies for Internet-of-Things: a comparative review," *IEEE Internet Things J.*, vol. 6, no. 2, pp. 2225-2240, Apr. 2019.

[4] L. Zhen et al., "Optimal preamble design in spatial group-based random access for satellite-M2M communications," *IEEE Wireless Commun. Lett.*, vol. 8, no. 3, pp. 953-956, Jun. 2019.

[5] Q. Yang and S. Yoo, "Optimal UAV path planning: sensing data acquisition over IoT sensor networks using multi-objective bio-inspired algorithms," *IEEE Access*, vol. 6, pp. 13671-13684, 2018.

[6] J. Baek, S. I. Han and Y. Han, "Energy-efficient UAV routing for wireless sensor networks," *IEEE Trans. Veh. Technol.*, doi: 10.1109/TVT.2019.2959808

[7] J. Lyu, Y. Zeng and R. Zhang, "UAV-aided offloading for cellular hotspot," *IEEE Trans. Wireless Commun.*, vol. 17, no. 6, pp. 3988-4001, Jun. 2018.

[8] M. B. Pandian, M. L. Sichitiu and H. Dai, "Optimal resource allocation in random access cooperative cognitive radio networks," *IEEE Trans. Mobile Comput.*, vol. 14, no. 6, pp. 1245-1258, Jun. 2015.

[9] U. Raza, P. Kulkarni and M. Sooriyabandara, "Low Power Wide Area Networks: An Overview," *IEEE Commun. Survey & Tut.*, vol. 19, no. 2, pp. 855-873, Secondquart. 2017.

[10] M. Centenaro, L. Vangelista, A. Zanella and M. Zorzi, "Long-range communications in unlicensed bands: the rising stars in the IoT and smart city scenarios," *IEEE Wireless Commun.*, vol. 23, no. 5, pp. 60-67, Oct. 2016.

[11] S. Popli, R. K. Jha and S. Jain, "A Survey on Energy Efficient Narrowband Internet of Things (NBIoT): Architecture, Application and Challenges," *IEEE Access*, vol. 7, pp. 16739-16776, 2019.

[12] M. De Sanctis, E. Cianca, G. Araniti, I. Bisio and R. Prasad, "Satellite communications supporting Internet of Remote Things," *IEEE Internet Things J.*, vol. 3, no. 1, pp. 113-123, Feb. 2016.

[13] S. Maleki et al., "Cognitive spectrum utilization in Ka band multibeam satellite communications," *IEEE Commun. Mag.*, vol. 53, no. 3, pp. 24-29, Mar. 2015.

[14] M. Á. Vázquez, L. Blanco and A. I. Pérez-Neira, "Hybrid analog–digital transmit beamforming for spectrum sharing backhaul networks," *IEEE Trans. Signal Process.*, vol. 66, no. 9, pp. 2273-2285, May 2018.

[15] A. H. Khan, M. A. Imran and B. G. Evans, "Semi-adaptive beamforming for OFDM based hybrid terrestrial-satellite mobile system," *IEEE Trans. Wireless Commun.*, vol. 11, no. 10, pp. 3424-3433, Oct. 2012.

[16] C. Liu, W. Feng, Y. Chen, C.-X. Wang and N. Ge, "Optimal beamforming for hybrid satellite terrestrial networks with nonlinear PA and imperfect CSIT," *IEEE Wireless Commun. Lett.*, doi: 10.1109/LWC.2019.2952124.

[17] Y. Zeng and R. Zhang, "Energy-efficient UAV communication with trajectory optimization," *IEEE Trans. Wireless Commun.*, vol. 16, no. 6, pp. 3747-3760, Jun. 2017.

[18] Y. Chen, W. Feng, and G. Zheng, "Optimum placement of UAV as relays," *IEEE Commun. Lett.*, vol. 22, no. 2, pp. 248-251, Feb. 2018.

[19] C.-X. Wang, J. Bian, J. Sun, W. Zhang, and M. Zhang, "A survey of 5G channel measurements and models," *IEEE Commun. Surveys Tuts.*, vol. 20, no. 4, pp. 3142–3168, 4th Quart., 2018.

[20] H. Chang, J. Bian, C.-X. Wang, Z. Bai, W. Zhou, and H. Aggoune, "A 3D non-stationary wideband GBSM for low-altitude UAV-to-ground V2V MIMO channels," *IEEE Access*, vol. 7, no. 1, pp. 70719-70732, Dec. 2019.

[21] C. Liu, W. Feng, J. Wang, Y. Chen and N. Ge, "Aerial small cells using coordinated multiple UAVs: an energy efficiency optimization perspective," *IEEE Access*, vol. 7, pp. 122838-122848, 2019.

[22] X. Wang, W. Feng, Y. Chen and N. Ge, "UAV swarm-enabled aerial CoMP: a physical layer security perspective," *IEEE Access*, vol. 7, pp. 120901-120916, 2019.

[23] M. Hua, Y. Wang, M. Lin, C. Li, Y. Huang and L. Yang, "Joint CoMP transmission for UAV-aided cognitive satellite terrestrial networks," *IEEE Access*, vol. 7, pp. 14959-14968, 2019.

[24] J. Wang, C. Jiang, Z. Wei, C. Pan, H. Zhang and Y. Ren, "Joint UAV hovering altitude and power control for space-air-ground IoT networks," *IEEE Internet Things J.*, vol. 6, no. 2, pp. 1741-1753, Apr. 2019.

[25] ITU-R Recommendation, "Calculation of free-space attenuation," Int. Telecommun. Union, Geneva, Switzerland, ITU-R P. 525-4, 2019.

[26] ITU-R Recommendation, "Attenuation by atmospheric gases," Int. Telecommun. Union, Geneva, Switzerland, ITU-R P. 676-12, 2019.

[27] M. Monwar, O. Semiari and W. Saad, "Optimized path planning for inspection by Unmanned Aerial Vehicles swarm with energy constraints," *Proc. IEEE GLOBECOM*, Abu Dhabi, United Arab Emirates, 2018, pp. 1-6.

[28] O. M. Bushnaq, A. Celik, H. Elsawy, M. Alouini and T. Y. Al-Naffouri, "Aeronautical data aggregation and field estimation in IoT networks: hovering and traveling time dilemma of UAVs," *IEEE Trans. Wireless Commun.*, vol. 18, no. 10, pp. 4620-4635, Oct. 2019.

[29] Y. Zeng, Q. Wu and R. Zhang, "Accessing from the sky: a tutorial on UAV communications for 5G and beyond," *Proc. IEEE*, vol. 107, no. 12, pp. 2327-2375, Dec. 2019.

[30] Q. Wu, Y. Zeng and R. Zhang, "Joint trajectory and communication design for multi-UAV enabled wireless networks," *IEEE Trans. Wireless Commun.*, vol. 17, no. 3, pp. 2109-2121, Mar. 2018.

[31] W. Feng, Y. Wang, N. Ge, J. Lu, and J. Zhang, "Virtual MIMO in multicell distributed antenna systems: coordinated transmissions with large-scale CSIT," *IEEE J. Sel. Areas Commun.*, vol. 31, no. 10, pp. 2067–2081, Oct. 2013.

[32] S. Yan, L. Qi and M. Peng, "User access mode selection in satellite-aerial based emergency communication networks," *Proc. IEEE ICC Workshop*, Kansas City, MO, Jul. 2018, pp. 1-6.

[33] W. Feng, J. Wang, Y. Chen, X. Wang, N. Ge, and J. Lu, "UAV-aided MIMO communications for 5G Internet of Things," *IEEE Internet Things J.*, vol. 6, no. 2, pp. 1731-1740, Apr. 2019.

[34] S. Boyd and L. Vandenberghe, *Convex optimization*. Cambridge University Press, 2004.

[35] T. Wei, W. Feng, J. Wang, N. Ge, and J. Lu, "Exploiting the shipping lane information for energy-efficient maritime communications," *IEEE Trans. Veh. Tech.*, vol. 68, no. 7, pp. 7204–7208, Jul. 2019.

[36] W. Murray and M. L. Overton, "A projected Lagrangian algorithm for nonlinear minimax optimization," *SIAM J. Sci. Stat. Comput.*, vol. 1, no. 3, pp. 345-370, Sep. 1980.

[37] Z. Shen, J. G. Andrews and B. L. Evans, "Adaptive resource allocation in multiuser OFDM systems with proportional rate constraints," *IEEE Trans. Wireless Commun.*, vol. 4, no. 6, pp. 2726-2737, Nov. 2005.

[38] Y. Sun, P. Babu and D. P. Palomar, "Majorization-minimization algorithms in signal processing, communications, and machine learning," *IEEE Trans. Signal Process.*, vol. 65, no. 3, pp. 794-816, Feb.1, 2017.